



## Design, synthesis, and *in vitro* evaluation of 4-aminoalkyl-1 (2*H*)-phthalazinones as potential multifunctional anti-Alzheimer's disease agents

Chanyuan Ye<sup>1</sup>, Rui Xu<sup>1</sup>, Zhongcheng Cao, Qing Song, Guangjun Yu, Yichun Shi, Zhuoling Liu, Xiuxiu Liu<sup>\*</sup>, Yong Deng<sup>\*</sup>

Department of Medicinal Chemistry, Key Laboratory of Drug-Targeting and Drug Delivery System of the Education Ministry and Sichuan Province, Sichuan Engineering Laboratory for Plant-Sourced Drug and Sichuan Research Center for Drug Precision Industrial Technology, West China School of Pharmacy, Sichuan University, Chengdu 610041, China

### ARTICLE INFO

#### Keywords:

Alzheimer's disease  
4-(aminoalkyl)-1(2*H*)-phthalazinone derivatives  
Multifunctional agents  
Acetylcholinesterase inhibitors  
Monoamine oxidases inhibitors  
 $A\beta$  aggregation inhibitors  
Anti-neuroinflammation

### ABSTRACT

A series of 4-aminoalkyl-1(2*H*)-phthalazinone derivatives was designed and synthesized as potential multifunctional agents for Alzheimer's disease (AD) treatment. *In vitro* biological assay results demonstrated that most synthesized compounds exhibited significant AChE inhibition, moderate to high MAOs inhibitory potencies and good anti-platelet aggregation abilities. Among them, compound **15b** exhibited the highest inhibitory potencies towards MAO-B and MAO-A ( $IC_{50} = 0.7 \mu\text{M}$  and  $6.4 \mu\text{M}$  respectively), moderate inhibition towards AChE ( $IC_{50} = 8.2 \mu\text{M}$ ), and good activities against self- and  $\text{Cu}^{2+}$ -induced  $A\beta_{1-42}$  aggregation and platelet aggregation. Moreover, **15b** also displayed antioxidant capacity, neuroprotective potency, anti-neuroinflammation and BBB permeability. These excellent results indicated that compound **15b** could be worthy of further studies to be considered as a promising multifunctional candidate for the treatment of AD.

### 1. Introduction

Alzheimer disease (AD), the most common neurodegenerative disease, is the main cause of dementia. This slowly progressive disease is age-related and mainly affects people over 65 years old, and is characterised by memory and orientation loss, impaired judgement, language disturbances and behavioural changes [1,2]. It is estimated that there are over 50 million people living with dementia globally, a figure set to increase to 152 million by 2050, which has led to considerable implications along with the colossal financial burden on the families and society [3]. Although the exact cause of AD is still unclear, several pathological hallmarks such as  $\beta$ -amyloid ( $A\beta$ ) deposition, tau protein hyperphosphorylation and accumulation, decline in acetylcholine (ACh) levels, oxidative stress, biometal dyshomeostasis, astrogliosis and neuronal dystrophy are thought to play vital roles in the onset and progression of the disease [4].

The decrease of cholinergic transmission is considered to cause a series of clinical manifestations, mainly cognitive and memory dysfunction. Cholinesterase (ChE), a ubiquitous serine hydrolase

comprising two types: acetylcholinesterase (AChE) and butyrylcholinesterase (BuChE), can affect the activity of cholinergic neurons through hydrolyzing the acetylcholine (ACh). In addition, cholinergic can also regulate the synthesis and release of nerve growth factor (NGF) in the cerebral cortex and hippocampus, which further lead to the deposition of  $A\beta$ . Accordingly, cholinesterase inhibitors have been used to reduce the pathological ACh hydrolysis and the  $A\beta$  toxicity, thereby achieving the effect of AD treatment [4–6]. Several acetylcholinesterase inhibitors (AChEIs) approved by FDA, including donepezil, rivastigmine and galantamine, have been demonstrated to enhance cholinergic levels and improve cognitive dysfunction to some extent [7]. Therefore, inhibition towards AChE has been an attractive treatment strategy for AD. However, the above marketed AChEIs, unfortunately, can not change the pathological process and reverse the condition of AD due to its complex etiology, and more single-target drugs in the clinical research stage have been reported failures one after another [8]. As a consequence, more researches have paid attention to applying “multi-target-directed ligands” (MTDLs) to AD treatment [9].

Monoamine oxidase (MAO), mitochondrial membrane flavoenzyme

<sup>\*</sup> Corresponding authors.

E-mail addresses: [liuxiuxiu@scu.edu.cn](mailto:liuxiuxiu@scu.edu.cn) (X. Liu), [dengyong@scu.edu.cn](mailto:dengyong@scu.edu.cn) (Y. Deng).

<sup>1</sup> These authors contributed equally to this work.

existing in two different isoforms (MAO-A and -B), is responsible for oxidative deamination of major xenobiotic amines and monoamine neurotransmitters to regulate their concentration and metabolism in the brain and peripheral tissues [4,10]. It is noteworthy that the MAO-B expression was increased in the cerebral cortex and the hippocampus regions of AD patients, and activation of the MAO-B was also associated with disruption of cholinergic neurons, formation of  $A\beta$  plaques, and NFTs, further contributing to the etiology of AD [11]. In addition, it is known that MAO-A inhibitors have been used as antidepressant agents, which may be helpful to relieve depressive symptoms in AD patients [12]. Moreover, the overexpression of MAOs in the nerve tissue facilitates the generation of excessive  $H_2O_2$  and toxic free radicals, which enhance the oxidative stress and further produce reactive oxygen species (ROS), thereby causing the death of neurons in the brain. These processes play an important role in neurodegenerative diseases, such as AD and Parkinson disease (PD) [13]. Therefore, drugs with inhibitory potencies towards MAOs (especially MAO-B), antioxidant properties and neuroprotective potencies may have a positive effect on the treatment of AD [14].

$A\beta$  are derived from  $\beta$ -amyloid precursor protein (APP), a transmembrane glycoprotein, via the proteolytic functions of  $\beta$ -secretase (BACE1) and  $\gamma$ -secretase [15]. Noteworthy,  $A\beta$  (especially  $A\beta_{1-42}$ ) are prone to aggregate into  $\beta$  sheet conformations in the form of higher-order oligomers, protofibrils, and fibrils, which have been broadly examined in AD brain. Deposition of  $A\beta$  initiated a cascade of biochemical processes of AD pathogenesis, thereby leading to severe neurodegeneration or neuronal death [15–17]. Therefore, inhibition and clearance of  $A\beta_{1-42}$  aggregation may be a potent therapeutic strategy

for AD. In addition, some evidence indicated that a large amount of APP and a complete enzyme system that can hydrolyze APP to  $A\beta$  were found in platelets [18]. Activated platelets are the main source of  $A\beta$  in the blood. Simultaneously,  $A\beta$  deposited on the blood vessel wall also activates platelets in turn, thereby leading to a vicious cycle. Moreover, excessive  $A\beta$  can damage blood vessels, which may further cause the deposition of  $A\beta$  in the brain and cerebral blood vessels, ultimately promoting the occurrence and development of AD [19]. According to these, inhibiting platelet aggregation in brain tissue may be helpful for preventing AD and changing its course.

Besides, brain tissue damage caused by neuroinflammation, an important pathological change in AD patients, is mainly related to microglia, astrocytes and inflammatory factors [20,21]. Microglia activated by  $A\beta$  stimulation is considered to produce a large number of neurotoxic substances such as inflammatory factors and free radicals, including tumor necrosis factor (TNF- $\alpha$ ), interferon  $\gamma$  (INF- $\gamma$ ), ROS and so on. These neurotoxic substances induce neuroinflammation, neurons damage and the production of complement components, leading to autoimmune reactions, which in turn cause cognitive dysfunction and neuron loss. In addition, TNF- $\alpha$  and INF- $\gamma$  can also reduce the content of insulin degrading enzymes, the key enzymes for  $A\beta$  degradation, thereby increasing  $A\beta$  deposition [22,23]. The above findings suggest that anti-inflammatory drugs may be promising candidates for AD treatment.

It is reported that phthalazinone derivatives showed a wide range of biological activities such as AChE inhibition,  $A\beta_{1-42}$  aggregation inhibition, anti-platelet aggregation, and other potencies including antioxidant, anti-inflammatory, anti-depressant and protective effect on PC12 injury induced by  $H_2O_2$  with low hepatotoxicity [24–26], which

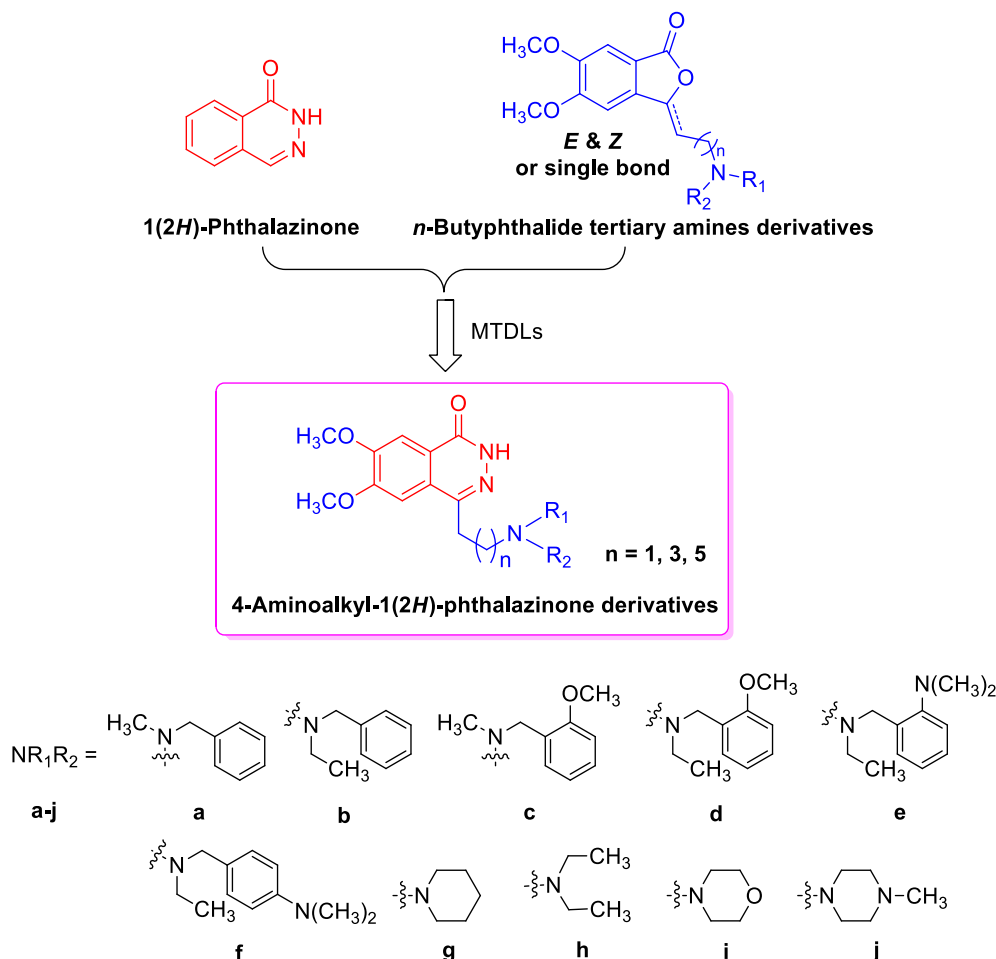


Fig. 1. Design strategy for 4-aminoalkyl-1(2H)-phthalazinone derivatives.

suggested that such derivatives may play an important role in AD therapy. In addition, our group had reported a series of phthalide alkyl tertiary amine derivatives (Fig. 1) with MTDLs' profiles [27]. These derivatives showed excellent AChE inhibition potencies ( $IC_{50}$  values ranging from 2.66 nM to 24.9  $\mu$ M) and good anti-oxidant activities expressed as ORAC values from 0.31 to 3.64-fold of Trolox. Unfortunately, this series of derivatives only exhibited weak  $A\beta_{1-42}$  aggregation inhibition and low MAOs inhibitory potencies. Therefore, based on our previously reported scaffold (Fig. 1, phthalide alkyl tertiary amine derivatives), we replaced the phthalide nucleus with phthalazinone moiety (Fig. 1, 1(2*H*)-phthalazinone) to optimize their multi-target anti-AD potentials. To this end, eighteen candidates of 4-aminoalkyl-1(2*H*)-phthalazinone derivatives containing carbon chains of different length and terminal tertiary amines were designed, synthesized and expected to possess excellent inhibition of AChE, enhanced inhibition of MAOs,  $A\beta_{1-42}$  aggregation and platelet aggregation, biological activities of antioxidant, anti-inflammatory and neuroprotective, and proper BBB permeability simultaneously as balanced and multifunctional agents for AD therapy.

## 2. Results and discussion

### 2.1. Chemistry

The synthetic route of intermediates **3a**, **3b** and **7** is shown in Scheme 1. Commercially available  $\alpha,\omega$ -diols **1a** or **1b** was reacted with benzoyl chloride to obtain  $\alpha,\omega$ -diol benzoic acid monoesters **2a** or **2b** [28]. Treating compounds **2a** or **2b** with 2,4,6-trichloro-1,3,5-triazine and DMSO in the presence of triethylamine afforded the corresponding benzoyloxyalkyl aldehyde **3a** or **3b** [29]. In addition, the reaction of 5,6-dimethoxyphthalide (**4**) with *N*-bromosuccinimide, using AIBN as initiator, afforded the compound **5**, which then was hydrolyzed to provide **6** [30]. Then, compound **6** was reacted with  $P(OEt)_3$  in the presence of  $Py \cdot HClO_4$  to give the intermediate **7** [31].

As the intermediates **3a**, **3b** and **7** in hand, the designed compounds were obtained according to Scheme 2. Compound **3a** or **3b** was condensed with **7** via the Horner-Wadsworth-Emmons reaction, using NaOH as base to yield the corresponding intermediate **8a** or **8b** [32], then followed by aminolysis reaction to get **9a** or **9b** [33]. Subsequently, compound **9a** or **9b** was hydrolyzed with  $K_2CO_3$  in a mixed solution of methanol and water to obtain alkyl alcohol **10a** or **10b**, which was then reacted with benzenesulfonylchloride to provide the benzenesulfonyl ester **11a** or **11b**, respectively. Then, substitution of these benzenesulfonyl esters with a series of secondary amines **12a-j** in the presence of  $K_2CO_3$  gave the corresponding key intermediates **13a-j** or **14a-f** [34]. Finally, the target products **15a-j** and **16a-f** were obtained by the reaction of these key intermediates with hydrazine hydrate in ethanol [35].

As for target compounds **23a** and **23c**, the synthetic method is

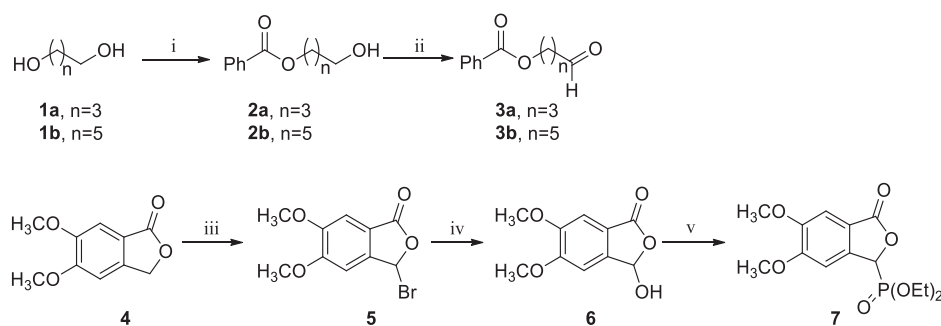
described in Scheme 3. The commercial 4,5-dimethoxyphthalic acid (**17**) was used as starting material. The intramolecular dehydration of **17** gave 4,5-dimethoxyphthalic anhydride (**18**), then reacted with ethyl 2-(triphenylphosphinidene)acetate to provide compound **19** via Wittig reaction [36,37]. Synthesis of **20** was carried out using **19** and hydrazine hydrate as reactants [38], and subsequently reduced with sodium borohydride in the presence of LiCl to give intermediate **21** [39], which then reacted with thionyl chloride to obtain the chlorinated product **22** [40]. Finally, compound **22** was condensed with the corresponding secondary amines using tetrabutylammonium bromide (TBAB) as phase transfer catalyst in acetonitrile to provide the target products **23a** and **23c**. The standard techniques including  $^1H$  NMR,  $^{13}C$  NMR and ESI-MS were used to characterize the chemical structure of all target products. And the purity of all the target compounds was determined by high-performance liquid chromatography (HPLC) analysis to be over 97.0%.

### 2.2. Pharmacology

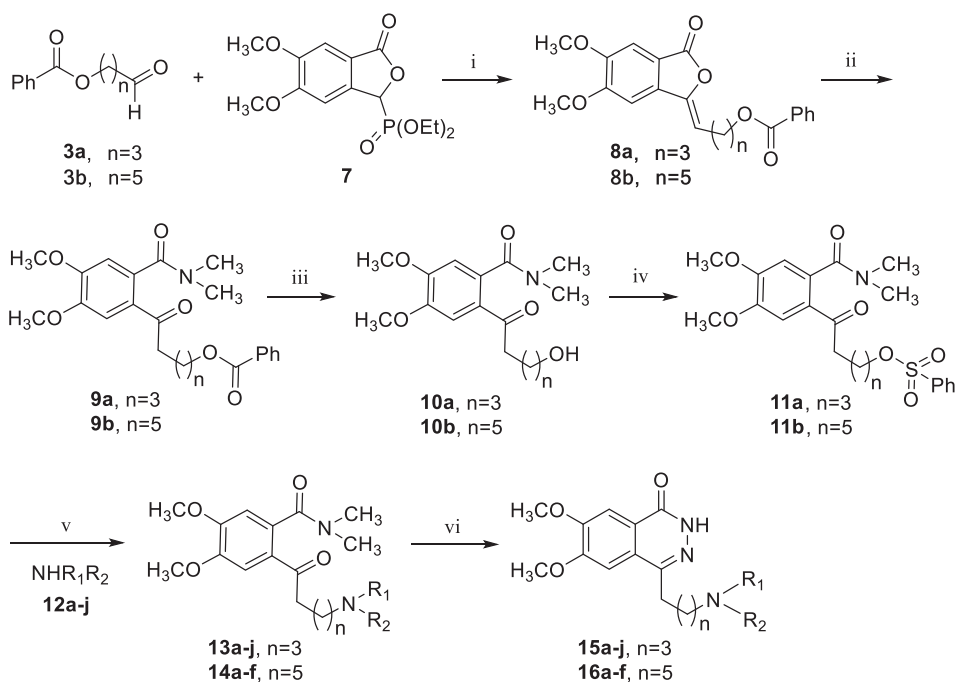
#### 2.2.1. AChE and BuChE inhibition

The 4-aminoalkyl-1(2*H*)-phthalazinone derivatives **15**, **16** and **23** were examined by modified Ellman's method for their *in vitro* inhibitory potencies against AChE (from *electric eel*, EeAChE) and BuChE (from rat serum, RatBuChE), and their potencies were compared to the well-known AChE inhibitors, donepezil and rivastigmine [41]. In order to clarify the effect of phthalazinone nucleus on ChE inhibitory potency, the key intermediates **13a**, **13c**, **13e**, **13f** and **13i** were also evaluated for their ChE inhibitory potencies. The ChE inhibitory results were expressed as  $IC_{50}$  values or percent inhibition rates, which were presented in Table 1.

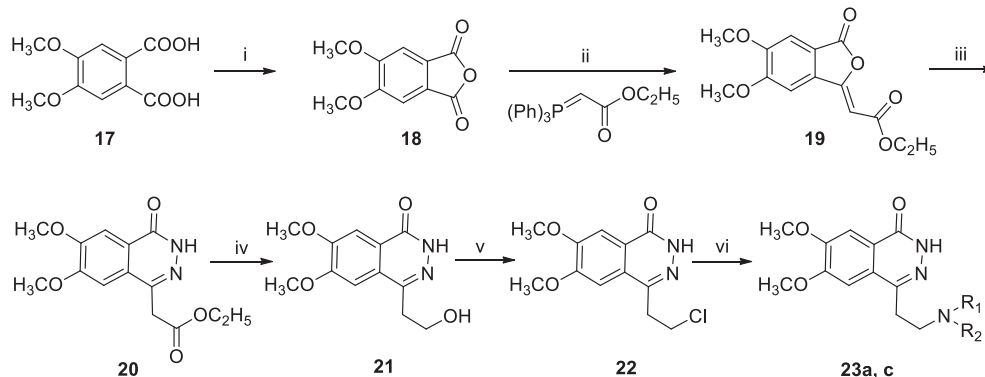
All synthesized target compounds showed potent and selective inhibitory potencies towards AChE over BuChE. Especially, the activities of **16a**, **16b**, **16c**, **16d** and **16e** are particularly excellent with the  $IC_{50}$  values as 0.10  $\mu$ M, 0.16  $\mu$ M, 0.47  $\mu$ M, 0.68  $\mu$ M and 0.45  $\mu$ M, respectively. Although they showed lower inhibitory effect than donepezil ( $IC_{50}$  = 0.078  $\mu$ M), most of the synthesized compounds were still more excellent than rivastigmine ( $IC_{50}$  = 25.81  $\mu$ M) for AChE inhibition. Through the structure-activity relationship (SAR) analysis, we could find that there are three important factors affecting the inhibition of AChE, including the presence of phthalazinone moiety, the length of the methylene side chain and terminal tertiary amine species. As shown in Table 1, compared with the compounds **15a-j**, **16a-f**, **23a** and **23c**, the intermediates **13a-f** without the phthalazinone moiety showed much lower or almost no AChE inhibitory potency. It indicated that the presence of phthalazinone moiety was crucial for the inhibition of AChE, which was consistent with our design strategy. Besides, the activities of the compounds with six methylene moieties as the side chains (**16a-f**) exhibited higher than that of the compounds containing four (**15a-j**), and compound **23a** or **23c** with two methylene moieties exhibited lowest AChE inhibition when it comes to the same terminal tertiary



**Scheme 1.** Synthesis of intermediates **3a**, **3b** and **7**. Reagents and conditions: (i)  $PhCOCl$ ,  $Et_3N$ , THF, 50 °C for 3 h, yield 86.0%(**2a**), 92.3%(**2b**); (ii) 2,4,6-trichloro-1,3,5-triazine,  $Et_3N$ , DMSO, THF, -30 °C for 2 h then rt for 2 h, yield 85.2%(**3a**), 90.5%(**3b**); (iii) NBS, AIBN,  $PhCl$ , 70 °C for 3 h, yield 78.2%; (iv)  $H_2O$ , reflux for 2 h, yield 65.8%; (v)  $P(OEt)_3$ ,  $Py \cdot HClO_4$ ,  $CHCl_3$ , rt for overnight, yield 80.5%.



**Scheme 2. Synthesis of compounds 15a-j and 16a-f.** Reagents and conditions: (i) NaOH, CH<sub>2</sub>Cl<sub>2</sub>, rt for 3 h; (ii) HN(CH<sub>3</sub>)<sub>2</sub>·HCl, Et<sub>3</sub>N, EtOH, reflux for 3 h, yield 76.5%(9a), 75.4%(9b) (two-steps); (iii) K<sub>2</sub>CO<sub>3</sub>, CH<sub>3</sub>OH, H<sub>2</sub>O, rt for 15 h, yield 81.3%(10a), 78.6%(10b); (iv) benzenesulfonylchloride, Et<sub>3</sub>N, CH<sub>2</sub>Cl<sub>2</sub>, rt for overnight, yield 89.4%(11a), 92.0%(11b); (v) NHR<sub>1</sub>R<sub>2</sub> (12a-j), K<sub>2</sub>CO<sub>3</sub>, CH<sub>3</sub>CN, 50 °C for 5 ~ 7 h, yield 62.2 ~ 73.1%; (vi) N<sub>2</sub>H<sub>4</sub>·H<sub>2</sub>O, EtOH, reflux for 8 ~ 10 h, yield 50.1 ~ 62.2%.



**Scheme 3. Synthesis of compounds 23a and 23c.** Reagents and conditions: (i) Ac<sub>2</sub>O, THF, reflux for 4 h, yield 94.8%; (ii) Toluene, 80 °C for 3 h, yield 89.0%; (iii) N<sub>2</sub>H<sub>4</sub>·H<sub>2</sub>O, EtOH, reflux for 3 h, yield 83.0%; (iv) NaBH<sub>4</sub>, LiCl, EtOH, THF, rt for overnight, yield 80.1%; (v) SOCl<sub>2</sub>, DMF, CHCl<sub>3</sub>, reflux for 10 h, yield 89.2%; (vi) NHR<sub>1</sub>R<sub>2</sub>, K<sub>2</sub>CO<sub>3</sub>, TBAB, CH<sub>3</sub>CN, reflux for 10 h, yield 62.1 ~ 63.2%.

amine species. Thus, it could be speculated that in the compound **23a** or **23c**, the length of two methylenes side chain is too short to bind to the catalytic active site (CAS) and the peripheral anionic site (PAS) of the enzyme simultaneously. In addition, based on the displayed data, we could find that compounds with benzylamine side chains (**15a-f**) showed higher activities against AChE than those with the aliphatic amines side chains (**15g-j**) in general. Besides, it seems that derivatives having *N*-(2-dimethylamino)benzyl group moiety (**15e**, **16e**) showed higher anti-AChE activities in comparison to those having *N*-(4-dimethylamino)benzyl group (**15f**, **16f**). Furthermore, the anti-AChE activities of tested compounds slightly increased when the *N*-ethyl group connected to the end of the carbon chain (**15b**, **16b**, **16d**) was replaced by *N*-methyl structure (**15a**, **16a**, **16c**). Concerning BuChE inhibition, the inhibitory effect of the synthesized compounds was weaker than their corresponding anti-AChE potency, showing selective inhibition towards AChE over BuChE. In conclusion, the ChE inhibition assay results indicated that our designed 4-aminoalkyl-1(2*H*)-phthalazinone derivatives may be a potent AChE inhibitor and beneficial for the compounds' multi-target and balanced anti-AD function.

### 2.2.2. Kinetic study for the inhibition of AChE

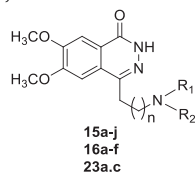
In order to investigate the mechanism of AChE inhibition, compound **15b** was used for a kinetic study with *Ee*AChE as a substrate and Lineweaver-Burk curves were showed as Fig. 2 [42]. According to the results, it could be observed that both slopes and vertical intercepts increased, which means that  $K_m$  values decreased and  $V_{max}$  increased at an increasing concentration of **15b**, and simultaneously, the curves intersected in the second quadrant of the coordinate axis. Thus, the above results indicated that compound **15b** might be a mixed-type inhibitor of AChE and it could bind to both the CAS and PAS sites of AChE. In addition, a plot of the slope versus the inhibitor's concentration afforded the inhibition constant  $K_i$  for compound **15b** as 4.06  $\mu$ M.

### 2.2.3. Molecular modeling study

The results above at the enzyme level were in accordance with our design strategy, which prompted us to further investigate the potential binding modes of the ligand **15b** with its target acetylcholinesterase (Fig. 3A). The reported X-ray crystal structure of *Tc*AChE (PDB code: 1EVE) was chosen for our molecular modeling study using the docking program, AutoDock 4.2 package. And the docking result compared with

**Table 1**

In vitro inhibition of *Ee*AChE, *Rat*BuChE and MAOs by 4-aminoalkyl-1(2*H*)-phthalazinone derivatives **15**, **16**, **23**, intermediates **13** and reference compounds.



Compd.	n	NR <sub>1</sub> R <sub>2</sub>	IC <sub>50</sub> (μM) ± SD <sup>a</sup> or % Inhibition <sup>b</sup>			
			<i>Ee</i> AChE <sup>c</sup>	<i>Rat</i> BuChE <sup>d</sup>	MAO-A	MAO-B
<b>13a</b>	3		8.0%	n.a. <sup>e</sup>	12.1%	25.9%
<b>13c</b>	3		6.4%	n.a. <sup>e</sup>	17.7%	12.4%
<b>13e</b>	3		n.a. <sup>e</sup>	6.9%	6.1%	8.5%
<b>13f</b>	3		n.a. <sup>e</sup>	6.8%	26.0%	10.4%
<b>13i</b>	3		n.a. <sup>e</sup>	n.a. <sup>e</sup>	18.4%	19.6%
<b>15a</b>	3		8.0 ± 0.2	9.6%	21.9%	25.0%
<b>15b</b>	3		8.2 ± 0.2	8.9%	6.4 ± 0.2	0.7 ± 0.1
<b>15c</b>	3		7.4 ± 0.3	6.6%	18.0%	10.5%
<b>15d</b>	3		7.3 ± 0.1	7.8%	23.5%	32.2%
<b>15e</b>	3		9.0 ± 0.2	5.4%	21.0%	17.9%
<b>15f</b>	3		12.6 ± 0.2	n.a. <sup>e</sup>	37.7%	3.6 ± 0.2
<b>15 g</b>	3		26.3%	n.a. <sup>e</sup>	19.8%	45.8%
<b>15 h</b>	3		25.4%	n.a. <sup>e</sup>	15.6%	37.5%
<b>15i</b>	3		10.4%	n.a. <sup>e</sup>	14.9%	28.5%
<b>15j</b>	3		32.8%	n.a. <sup>e</sup>	13.7%	5.0 ± 0.1
<b>16a</b>	5		0.1 ± 0.1	14.0%	9.8%	38.9%
<b>16b</b>	5		0.2 ± 0.1	31.1%	21.3%	36.2%
<b>16c</b>	5		0.5 ± 0.1	9.2%	22.3%	48.3%
<b>16d</b>	5		0.7 ± 0.1	11.1%	21.5%	46.2%
<b>16e</b>	5		0.5 ± 0.1	15.9%	25.9%	34.1%
<b>16f</b>	5		6.3 ± 0.1	n.a. <sup>e</sup>	24.7%	32.5%
<b>23a</b>	1		28.1%	n.a. <sup>e</sup>	6.9%	15.7%
<b>23c</b>	1		32.3%	n.a. <sup>e</sup>	5.5%	34.8%
Donepezil	—	—	0.08 ± 0.001	22.6 ± 0.1	NT <sup>f</sup>	NT <sup>f</sup>
Rivastigmine	—	—	25.8 ± 1.2	8.2 ± 0.1	NT <sup>f</sup>	NT <sup>f</sup>
Clorgyline	—	—	NT <sup>f</sup>	NT <sup>f</sup>	0.003 ± 0.0005	2.4 ± 0.1
Rasagiline	—	—	NT <sup>f</sup>	NT <sup>f</sup>	2.6 ± 0.02	0.01 ± 0.0007
Iproniazid	—	—	NT <sup>f</sup>	NT <sup>f</sup>	0.8 ± 0.01	0.98 ± 0.03

<sup>a</sup> IC<sub>50</sub> values represent the concentration of inhibitor required to decrease enzyme activity by 50% and are the mean of three independent experiments, each performed in triplicate. Data were expressed as mean ± SD (SD = standard deviation).

<sup>b</sup> Percentages are the percent inhibition of ChE or MAO by tested compounds at 10 μM.

<sup>c</sup> AChE from *Electrophorus electricus*.

<sup>d</sup> BuChE from rat serum.

<sup>e</sup> n.a. = no active. Compounds defined “no active” means that percent inhibition is < 5.0% at a concentration of 10 μM in the assay conditions.

<sup>f</sup> NT = not tested.

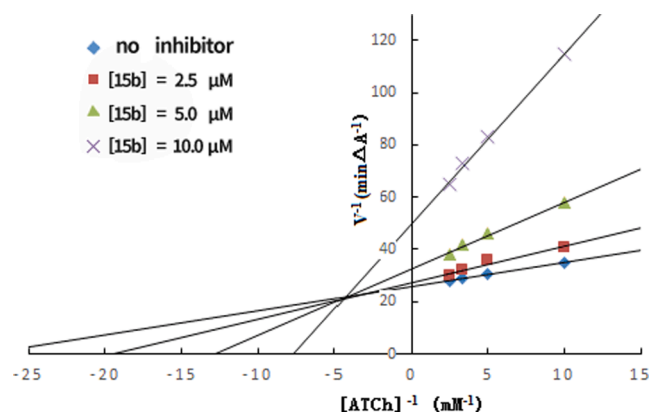


Fig. 2. Kinetic study on the mechanism of *EeAChE* inhibition by compound **15b**. Merged Lineweaver-Burk reciprocal plots of AChE initial velocity with increasing substrate concentration (0.1–0.4 mM) in the absence or presence of **15b**. Lines were derived from a weighted least-squares analysis of data points.

the donepezil molecule was shown in Fig. 3B. In addition, in order to interpret and verify our result that the inhibition towards AChE was affected by the length of the carbon chain mentioned in section 2.2.1, we also conducted a docking experiment of compound **16b**. The results were shown in Fig. 4. The molecular docking results provided a reasonable explanation for the excellent AChE inhibitory potency of 4-aminoalkyl-1(2*H*)-phthalazinone derivatives. As shown in Fig. 3A, compound **15b** bound perfectly to AChE and occupied the entire enzymatic CAS, the mid-gorge site and the PAS. In the *TcAChE*-**15b** complex, various of intermolecular interactions were observed. The 2-position amide of compound **15b** interacted with Phe331 via a strong intermolecular hydrogen bond. Simultaneously, the phthalazinone moiety and *N*-benzylethylamine moiety of **15b** formed parallel  $\pi$ - $\pi$  stacking interaction with Trp279 and Tyr70, respectively. Besides, hydrophobic bonds could be observed between 4-position methylene side chain moiety and various residues including Tyr121, Tyr334 and Phe330. Furthermore, compounds **15b** also exhibited a potential hydrophobic interaction with residues Ile287, Gly335, Leu332, Asp72, Ser81, Trp84, and Asn85. The docking results was consistent with the kinetic study, which further verified that compound **15b** could simultaneously bind to the CAS and

PAS sites of AChE as a dual-site AChE inhibitor. In addition, the similar binding modes with *TcAChE* could be observed from the conformational overlap of the compound **15b** and donepezil (Fig. 3B), which also confirmed our previous experimental results. Besides, according to the docking result of compound **16b** with AChE (Fig. 4), we could find that the 2-position amide of **16b** also interacted with Phe331 via a strong hydrogen bond. Moreover, the phthalazinone moiety and 5,6-dimethoxyphenyl structure of **16b** was observed to form parallel  $\pi$ - $\pi$  stacking interaction with Tyr334, and **16b** also interacted with more amino acids such as Phe288, Ser286 and Gln69. Furthermore, the combination of compound **16b** (estimated binding energy = -11.37 kcal/mol) with AChE was more compact than that of **15b** (estimated binding energy = -10.73 kcal/mol). In other words, compound **16b** occupied the CAS site, the active site of the “cavity” and the PAS site of the enzyme more firmly, which verified our previous result that the AChE inhibition of the compounds with six methylene side chain were better than those of compounds with four.

#### 2.2.4. Inhibition of MAOs in vitro

To further evaluate the multifunctional biological profile of 4-aminoalkyl-1(2*H*)-phthalazinone derivatives, the recombinant human MAO-A and MAO-B were used to measure the MAOs inhibitory potencies of our designed derivatives with clorgyline, rasagiline and iproniazid as the positive controls [43]. The screening results were expressed as  $IC_{50}$  values or percent inhibition by tested compounds at 10  $\mu$ M. As shown in Table 1, all the designed derivatives exhibited MAOs inhibitory potencies of varying intensity. In particular, compound **15b** elicited outstanding and representative inhibitory potency towards both MAO-B ( $IC_{50}$  = 0.7  $\mu$ M) and MAO-A ( $IC_{50}$  = 6.4  $\mu$ M), and the MAO-B inhibitory effect was superior to the positive controls clorgyline ( $IC_{50}$  = 2.43  $\mu$ M) and iproniazid ( $IC_{50}$  = 0.98  $\mu$ M). In addition, compounds **15f** and **15j** also exhibited excellent MAO-B inhibitory potencies, with  $IC_{50}$  values as 3.6  $\mu$ M and 5.0  $\mu$ M, respectively. Besides, we could find that compounds with *N*-ethylbenzyl moiety (**15b**, **15d**) exhibited higher MAOs inhibition than those with *N*-methylbenzyl moiety (**15a**, **15c**) when it comes to four methylene moieties as the side chains, while there is no obvious law of the same kind when compounds with six methylene moieties were tested. Moreover, it is worth noting that the target derivatives (**15a-j**, **16a-f**, **23a**, **23c**) exhibited generally higher activities than the intermediates without the phthalazinone nuclear (**13a-e**) and also the lead

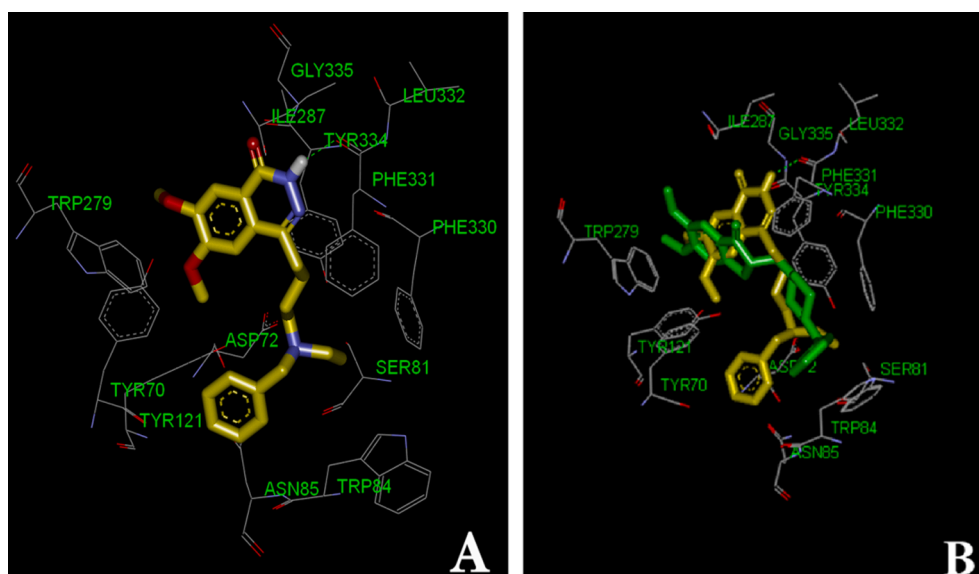
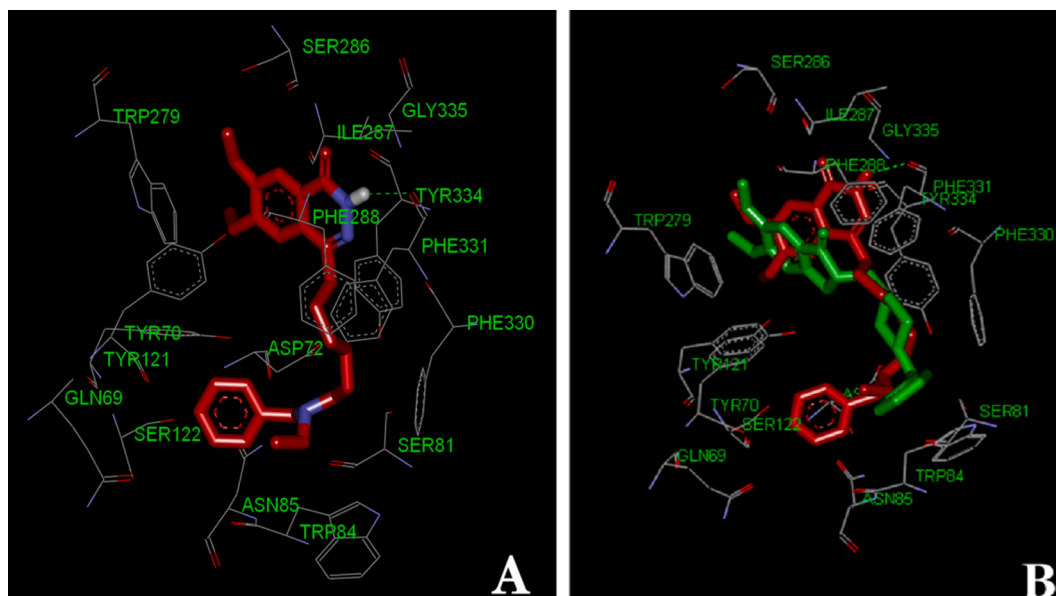


Fig. 3. Hypothetical binding mode (A) of compound **15b** interacting with residues in the binding site of *TcAChE* (PDB: 1EVE) and overlap (B) of compounds **15b** (yellow stick) and donepezil (green stick) interacting with residues in the binding site of *TcAChE* (PDB: 1EVE). The protein residues that participate in the main interactions with the inhibitor are labeled. (For interpretation of the references to colour in this figure legend, the reader is referred to the web version of this article.)



**Fig. 4.** Hypothetical binding mode (A) of compound **16b** interacting with residues in the binding site of TcAChE (PDB: 1EVE) and overlap (B) of compounds **16b** (red stick) and donepezil (green stick) interacting with residues in the binding site of TcAChE (PDB: 1EVE). The protein residues that participate in the main interactions with the inhibitor are labeled. (For interpretation of the references to colour in this figure legend, the reader is referred to the web version of this article.)

phthalide alkyl tertiary amine derivatives (Fig. 1, percent inhibition ranging from 1.09% to 38.8%) for inhibition of MAOs [27], which indicated that the phthalazinone moiety was beneficial to the improvement of MAOs inhibition.

#### 2.2.5. Molecular modeling studies of MAOs

To further study the hypothetical interactions with both isoforms of human MAOs, the most potent compound **15b** was chosen for docking simulations using the X-ray crystal structures of human MAO-A (PDB code: 2Z5X) and MAO-B (PDB code: 2V60). In MAO-A docking simulation (Fig. 5A), the phthalazinone moiety of compound **15b** was close to the coenzyme factor FAD and formed a parallel  $\pi$ - $\pi$  stacking interaction with the residue Tyr69. In addition, the 2-amide of compound **15b** could interact with residues Asn181 and Ile207 simultaneously to form two intermolecular hydrogen bonds, and the same interaction also existed between the 4-methoxy group of the ligand and residue Tyr407. Furthermore, it's worth noting that compound **15b** could interact with many other residues including Leu97, Val93, Gly110, Thr211, Ala111,

Cys323, Val210, Ser209, Ile325, Ile335, Ile480, Leu337, Phe208, Gln215, Met350, Phe352, Tyr444 and so on. As shown in Fig. 5B, the phthalazinone nucleus of **15b** was also close to the coenzyme factor FAD of MAO-B, and two intermolecular hydrogen bonds with residues Cys172 and Tyr407 could be observed. In addition,  $\pi$ - $\pi$  stacking interaction existed between ligand **15b** and residue Tyr407. Besides, it can be seen that **15b** also interacted with other residues such as Leu164, Leu167, Leu171, Leu328, Trp119, Pro102, Phe168, Phe343, Ile198, Ile199, Ile316, Gln206, Tyr60, Tyr326, Tyr398 and so on. Comparing Fig. 5A with Fig. 5B comprehensively, we can conclude that both MAO-A and MAO-B could be combined with **15b** very well, even if their combination methods were somewhat different. Indeed, it could be calculated by simulation that the binding energy of **15b** with MAO-A and MAO-B were  $-9.87$  kcal/mol and  $-11.76$  kcal/mol, respectively. In particular, according to the docking result of compound **15a** with MAO-B and overlap of compound **15a** and **15b** interacting with residues in the binding site of MAO-B (Supplementary Fig. S3 A/B), we could find that the phthalazinone nuclear of **15a** interacted with Cys172 via a

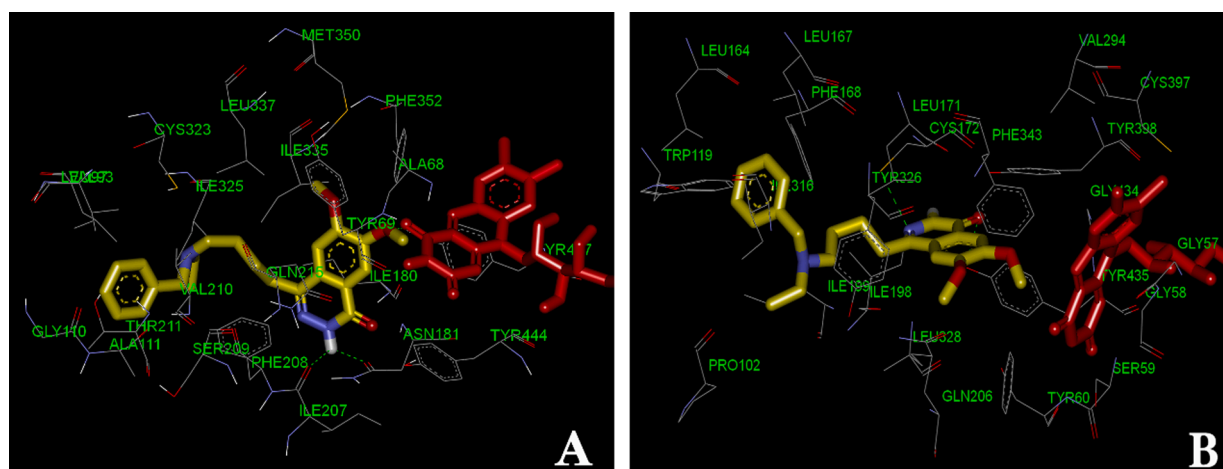


**Fig. 5.** Representation of compound **15b** docked into the binding sites of MAO-A (A) and -B (B), highlighting the protein residues that participate in the main interactions with the inhibitor. Ligand **15b** and FAD are displayed in yellow and red, respectively. Hydrogen-bonds are shown with the green dotted lines. (For interpretation of the references to colour in this figure legend, the reader is referred to the web version of this article.)

hydrogen bond, which means that **15b** has one more intermolecular hydrogen bond with residue Tyr407 of MAO-B than **15a**. Moreover, the combination of compound **15b** with MAO-B (estimated binding energy = -11.79 kcal/mol) was more compact than that of **15a** (estimated binding energy = -10.38 kcal/mol), which proves that the type of *N*-substituent on **15b** may be important for MAO-B inhibitory potency. In summary, the above data and analysis of the docking results interpreted these two facts well that compound **15b** exhibited excellent MAOs inhibitory potency and the inhibition towards MAO-B was stronger than MAO-A, which further confirmed the reliability of our study on the inhibition of MAOs *in vitro*.

### 2.2.6. Inhibition of self-induced $A\beta_{1-42}$ aggregation

$A\beta_{1-40}$  and  $A\beta_{1-42}$ , the two primary isoforms of  $A\beta$  peptide, play different roles in the pathogenesis of AD. Between them,  $A\beta_{1-42}$  is more prone to self-aggregation, thus forming oligomers with higher neurotoxicity than  $A\beta_{1-40}$  even if the amount of  $A\beta_{1-42}$  is much lower than  $A\beta_{1-40}$  [44]. Therefore,  $A\beta_{1-42}$  was selected to assess inhibitory effect of self-induced  $A\beta_{1-42}$  aggregation by our designed derivatives using the Thioflavin T (ThT) fluorescence assay, with curcumin as the positive control. The evaluation results were shown in Table 2. In general, most of the tested compounds exhibited moderate inhibitory percentages of self-induced  $A\beta_{1-42}$  aggregation, ranging from 20.9% to 36.2% at 25  $\mu$ M. In particular, compounds **15d**, **16a**, **16b** and **16c** provided better inhibitory activities (34.6%, 34.6%, 36.2% and 33.2% at 25  $\mu$ M, respectively), which were stronger than the lead phthalide alkyl tertiary amine derivatives (Fig. 1, percent inhibition ranging from 5% to 30% at 25  $\mu$ M) [27], but slightly weaker than curcumin (38.1% at 25  $\mu$ M). However, almost no significant change of inhibition rates could be observed when the length of the carbon chain or the tertiary amine structural fragments varied, which means that no obvious SAR existed for this series of compounds on the inhibition of self-induced  $A\beta_{1-42}$  aggregation.

### 2.2.7. Disaggregation of self-induced $A\beta_{1-42}$ aggregation fibrils

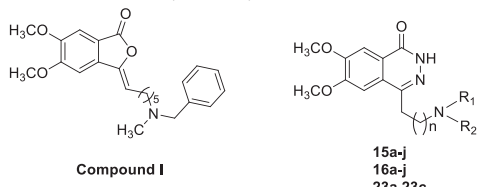
We chose some relatively high-activity target compounds as the representatives to investigate their disaggregation potency of self-induced  $A\beta_{1-42}$  aggregation fibrils. As shown in Table 2, all the tested compounds (25  $\mu$ M) manifested low to moderate inhibition rates ranging from 12.0% to 24.6%, compared with the reference compound curcumin (24.3% at 25  $\mu$ M). In particular, compounds **16b** and **16c** exhibited better disaggregation potency (23.2% and 24.6% at 25  $\mu$ M, respectively), equivalent to the positive control curcumin (24.3% at 25  $\mu$ M). However, there was also no obvious SAR could be found among these tested compounds on the disaggregation potency of self-induced  $A\beta_{1-42}$  fibrils, and their further dose-dependent experiment did not be conducted since the low disaggregation potency.

### 2.2.8. Inhibition of platelet aggregation

Several of literatures have reported that phthalazinone derivatives showed excellent inhibition of platelet aggregation, which was beneficial to the treatment of AD [45,46]. Therefore, the inhibitory potencies of platelet aggregation of our designed 4-aminoalkyl-1(2*H*)-phthalazinone derivatives were assessed by the classic turbidimetric method, using aspirin and *n*-butylphthalide (*dl*-NBP) as the positive controls. In addition, the anti-platelet aggregation potency of compound **I**, the typical compound of *n*-butylphthalide tertiary amines derivatives (Fig. 1), was also tested as a control for SAR analysis. According to the experimental results shown in Table 2, we could find that all the synthesized target compounds exhibited better inhibitory potencies of platelet aggregation ranging from 5.7% to 20.3%, compared with compound **I** (5.6% at 33  $\mu$ M), which indicated that the phthalazinone moiety was crucial for the anti-platelet aggregation potency of this new series of derivatives. Besides, most of the target compounds displayed good inhibitory potency, superior to the positive controls aspirin (9.4% at 33  $\mu$ M) and butylphthalide (6.1% at 33  $\mu$ M). Among these compounds, **23a** and **23c** possessed relatively stronger inhibitory ability

**Table 2**

Inhibition of platelet aggregation and self-induced  $A\beta_{1-42}$  aggregation, disaggregation of self-induced  $A\beta_{1-42}$  aggregation, oxygen radical absorbance capacity (ORAC, Trolox equivalents) by 4-aminoalkyl-1(2*H*)-phthalazinone derivatives **15**, **16**, **23** and reference compounds.



Compd.	% Inhibition of platelet aggregation <sup>a,f</sup>	% Inhibition of $A\beta_{1-42}$ aggregation <sup>b,c,f</sup>	% Disaggregation of $A\beta_{1-42}$ aggregation <sup>d,e,f</sup>	ORAC <sup>f,g</sup>
<b>15a</b>	16.1 ± 0.1	23.0 ± 0.1	13.3 ± 0.1	0.36 ± 0.02
<b>15b</b>	14.0 ± 0.2	31.7 ± 0.1	21.9 ± 0.1	0.49 ± 0.05
<b>15c</b>	14.8 ± 0.1	29.1 ± 0.1	22.2 ± 0.1	0.37 ± 0.01
<b>15d</b>	14.5 ± 0.2	34.6 ± 0.2	NT <sup>h</sup>	0.48 ± 0.04
<b>15e</b>	15.6 ± 0.1	27.9 ± 0.3	NT <sup>h</sup>	0.67 ± 0.03
<b>15f</b>	16.1 ± 0.1	29.5 ± 0.3	NT <sup>h</sup>	3.64 ± 0.06
<b>15 g</b>	9.8 ± 0.1	31.4 ± 0.1	NT <sup>h</sup>	0.32 ± 0.05
<b>15 h</b>	15.1 ± 0.2	20.9 ± 0.2	NT <sup>h</sup>	0.42 ± 0.09
<b>15i</b>	13.9 ± 0.2	22.3 ± 0.2	NT <sup>h</sup>	0.42 ± 0.01
<b>15j</b>	7.4 ± 0.1	28.5 ± 0.3	NT <sup>h</sup>	0.51 ± 0.05
<b>16a</b>	11.9 ± 0.1	34.6 ± 0.3	16.6 ± 0.1	0.42 ± 0.01
<b>16b</b>	9.2 ± 0.1	36.2 ± 0.3	23.2 ± 0.1	0.45 ± 0.05
<b>16c</b>	10.9 ± 0.1	33.2 ± 0.3	24.6 ± 0.2	0.43 ± 0.01
<b>16d</b>	9.2 ± 0.1	27.2 ± 0.2	NT <sup>h</sup>	0.45 ± 0.03
<b>16e</b>	5.7 ± 0.1	24.5 ± 0.2	NT <sup>h</sup>	0.55 ± 0.02
<b>16f</b>	9.9 ± 0.1	30.3 ± 0.2	NT <sup>h</sup>	3.16 ± 0.08
<b>23a</b>	20.3 ± 0.2	26.8 ± 0.2	12.0 ± 0.2	0.31 ± 0.02
<b>23c</b>	18.6 ± 0.3	26.5 ± 0.3	18.6 ± 0.2	0.32 ± 0.02
<i>dl</i> -NBP	6.1 ± 0.1	NT <sup>h</sup>	NT <sup>h</sup>	0.21 ± 0.01
aspirin	9.4 ± 0.1	NT <sup>h</sup>	NT <sup>h</sup>	NT <sup>h</sup>
curcumin	NT <sup>h</sup>	38.1 ± 0.1	24.3 ± 0.2	NT <sup>h</sup>
Compound <b>I</b>	5.6 ± 0.08	—	—	—

<sup>a</sup> Platelet from rat serum. Tested compounds were used at 33  $\mu$ M;

<sup>b</sup> For inhibition of self-induced  $A\beta$  aggregation, the thioflavin-T fluorescence method was used;

<sup>c</sup> Inhibition of self-induced  $A\beta_{1-42}$  aggregation by tested inhibitors at 25  $\mu$ M;

<sup>d</sup> For disaggregation of self-induced  $A\beta$  aggregation, the thioflavin-T fluorescence method was used;

<sup>e</sup> Disaggregation of self-induced  $A\beta_{1-42}$  aggregation by tested inhibitors at 25  $\mu$ M;

<sup>f</sup> The mean ± SD of the three independent experiments.

<sup>g</sup> Data are expressed as  $\mu$ M of Trolox equivalent/ $\mu$ M of tested compound;

<sup>h</sup> NT = not tested.

(20.3%, 18.6%, respectively) than others. Unfortunately, there was no obvious difference for inhibition of platelet aggregation could be observed among these tested compounds, which means that no more SAR existed among them on anti-platelet aggregation potency.

### 2.2.9. In vitro antioxidant potency assay

To further explore the multi-target biological potency of 4-aminoalkyl-1(2H)-phthalazinone derivatives, we used the well-established ORAC-FL method (oxygen radical absorbance capacity by fluorescein) with a water-soluble vitamin E analog (Trolox) as a standard to assess their abilities of scavenging radicals, equivalent to antioxidant activities. The evaluation results were expressed as Trolox equivalent and shown in Table 2. According to the displayed data, all the tested derivatives exhibited moderate to strong antioxidant activities with the ORAC values ranging from 0.31 to 3.6-fold of Trolox, superior to *dl*-NBP (ORAC value of 0.21 Trolox equivalent). Among them, the antioxidant potencies of **15f** and **16f** were particularly prominent with ORAC values as 3.6 and 3.2-fold Trolox equivalents, respectively, which suggested that the introduction of *N*-(4-dimethylaminobenzyl)ethylamine (**12f**) to the end of the linker was beneficial to improving the antioxidant potencies of the compounds. In addition, we could find that derivatives with *N*-4-dimethylamino group moiety (**15f**, **16f**) showed higher antioxidant activities in comparison to those having *N*-2-dimethylamino group (**15e**, **16e**), through which we could conclude that the position of dimethylamine substituent attached to the benzene ring is a crucial factor affecting the antioxidant capacities of tested compounds. However, almost no obvious SAR could be observed when the length of carbon chains and tertiary amine substituents species changed, which indicated that these two factors may have no significant influence on the antioxidant capacity of tested compounds.

### 2.2.10. Neuroprotective potency against H<sub>2</sub>O<sub>2</sub>-induced cell injury in PC12 cells

According to the above collected data, compounds **15b** and **16b** exhibited excellent and balanced multi-target activities for AD. Besides, compounds **15f** and **16f** showed the strongest antioxidant potencies, suggesting that they may be potential neuroprotective agents. Thus, these four representative compounds were selected as the most promising candidates of this small series for AD treatment, and worthy to be explored for their neuroprotective activities. It is reported that hydrogen peroxide (H<sub>2</sub>O<sub>2</sub>) is a metabolite in the body and a ROS that plays a key role in inducing PC12 cell damage [47]. Thus, the neuroprotection potentials of tested compounds at different concentrations (1 and 10 μM) were evaluated by cell viability assay with PC12 cells in the presence of H<sub>2</sub>O<sub>2</sub> containing 10% calf serum. Prior to the assessment of neuroprotective properties, PC12 cells were treated with **15b**, **16b**, **15f** and **16f** at 25 μM concentration. Cell viabilities of 97.5%, 99.0%, 97.3% and 98.6%, respectively, indicated that these compounds were not cytotoxic at the concentrations that were further used for neuroprotection assay. The subsequent measurement results were depicted in Fig. 6. Compared to the control group without treating H<sub>2</sub>O<sub>2</sub>, the cell viabilities of PC12

cells with H<sub>2</sub>O<sub>2</sub> (150 μM) decreased to 46% after incubated for 24 h. However, when compounds **15b**, **16b**, **15f** or **16f**, at the concentration of 1.0 μM, was added to the cells with H<sub>2</sub>O<sub>2</sub> respectively, the cell viabilities correspondingly increased to 64.3%, 63.9%, 73.8% or 72.4%. Furthermore, when the concentrations of the above compounds were increased to 10 μM, the cell viabilities further increased to 75.7%, 75.5%, 85.2% and 83.8%, respectively. Testing results clearly showed that the cell viability markedly increased when pretreated with increasingly concentrations of tested compounds, which further indicated that our designed compounds could effectively attenuate the damage of PC12 cells induced by H<sub>2</sub>O<sub>2</sub>, thereby exerting excellent neuroprotective activity.

### 2.2.11. In vitro anti-neuroinflammatory potency evaluation

As reported in the literature, neuroinflammation is closely related to the development of AD. The activation of microglia, as the main hallmark of neuroinflammation, leads to the release of various neurotoxic substances such as inflammatory cytokines and free radicals, thereby activating the immune inflammatory response and producing neurotoxicity [48–50]. Therefore, inhibition of the release of inflammatory cytokines and free radicals may play an important role in AD treatment. In this assay, **15b** and **16b** were selected as the representative compounds to investigate their anti-neuroinflammatory activities, which included the evaluation of interference induced by the cytotoxic effect of compound itself and the measurement on the production of inflammatory mediators NO and TNF-α in LPS-induced BV-2 microglial cells.

**2.2.11.1. Effect of compounds on survival rate of BV-2 cells.** The cytotoxicities of tested compounds were assessed by MTT assay [51]. As shown in Fig. 7, in the presence of different concentrations of **15b** or **16b** (0.5, 2.5 and 10.0 μM), the cell viability for BV-2 cells did not change significantly with or without lipopolysaccharide (LPS) as a stimulus, which indicated that both the tested compounds and LPS had no toxic effect on BV-2 cells.

**2.2.11.2. Evaluation of NO and TNF-α in LPS-stimulated BV-2 cells.** Inhibition of LPS-induced NO production was evaluated by Griess reaction method [52]. First, we evaluated the effect of different concentrations of tested compounds (0.5, 2.5 and 10.0 μM) on the release of NO in BV-2 cells without LPS. As shown in Fig. 8, the release volume of NO did not change significantly in the presence of tested compounds, which suggested that compounds themselves had no effect on the release of NO in BV-2 cells. Then a markedly increased production of NO could be observed when exposed to LPS (1 μg/mL). Noteworthy, pre-treatment with tested compounds (0.5, 2.5 and 10.0 μM) led to a markedly reduction of LPS-induced NO production, which expressed as the percent inhibition of 30.2%, 45.8% and 59.6%, respectively, for compound **15b**. In addition, the inhibition rates of representative compound **16b** were 24.8%, 41.4% and 50.5% at the above three concentrations respectively. To further investigate the effects of tested compounds on LPS-induced TNF-α production in BV-2 cells, the enzyme-linked immunosorbent assay (ELISA) was used to evaluate their ability of suppressing TNF-α levels [53]. Firstly, we measured the effect of tested compounds on the TNF-α production without the treatment of LPS. As displayed in Fig. 9, the release volume of TNF-α had no significantly change in test group compared with the control group, thus the compounds themselves had no effect on it. Then, we could find a markedly increase in TNF-α production when the cells were exposed to LPS (1 μg/mL) without tested compounds. Obviously, the compounds **15b** and **16b**, in the test group, exhibited effective inhibitory potencies towards TNF-α production in LPS-stimulated BV-2 cells in a concentration dependent way. The inhibition rates of **15b** at three concentrations of 0.5, 2.5 and 10.0 μM were 25.4%, 49.5% and 72.1%, respectively. The inhibition rates of **16b** at the concentrations of 0.5, 2.5 and 10.0 μM were 22.3%, 47.8% and 69.4%, respectively. In conclusion, both the representative compounds **15b** and

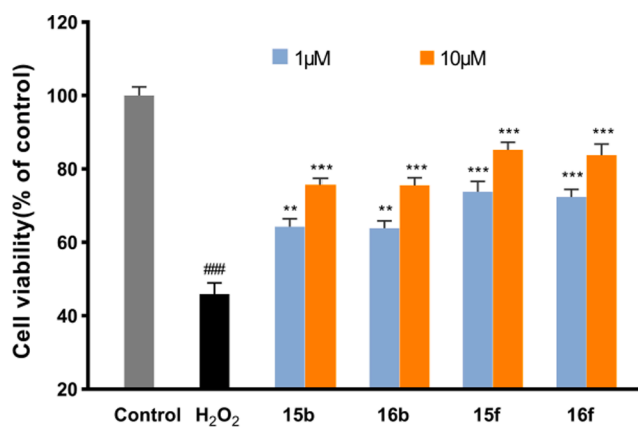


Fig. 6. Effects of compounds **15b**, **16b**, **15f** and **16f** on H<sub>2</sub>O<sub>2</sub>-induced PC12 cells injury (n = 3, mean ± SD; ####p < 0.001 versus control, \*\*p < 0.01 versus H<sub>2</sub>O<sub>2</sub>, \*\*\*p < 0.001 versus H<sub>2</sub>O<sub>2</sub>).

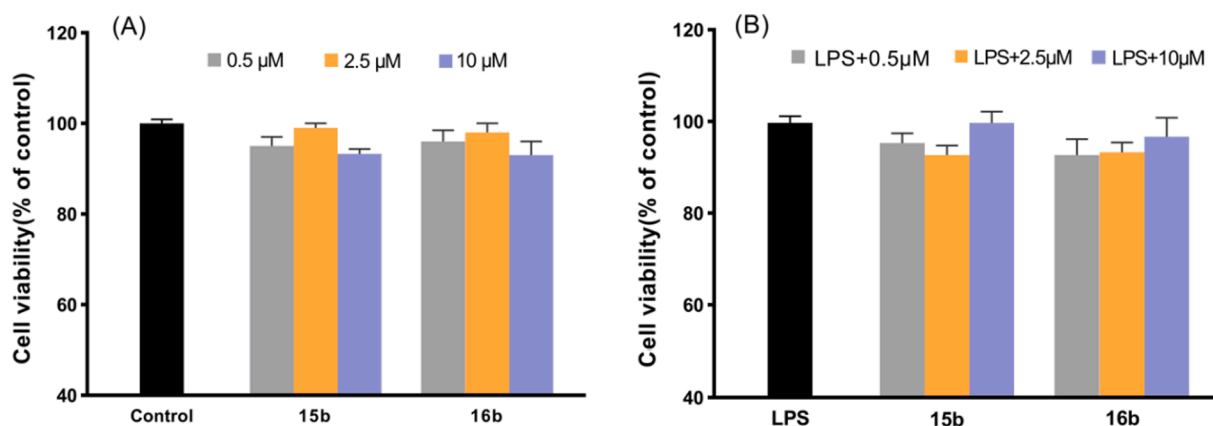


Fig. 7. Effects of compounds **15b** and **16b** without LPS. (A) or with LPS (1.0 µg/mL); (B) on the cell viability of microglia BV-2 cells. Cell viability was determined by MTT assay. The data are expressed as the mean ± SD from three independent experiments.

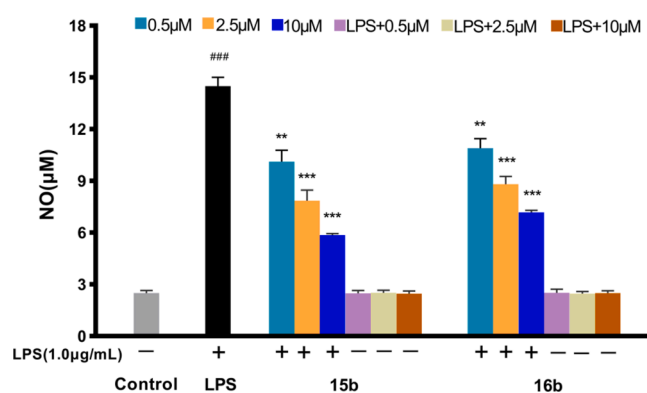


Fig. 8. Effects of compounds **15b** and **16b** on NO release in BV-2 cells and LPS-stimulated BV-2 cells (n = 3, mean ± SD; ###  $p < 0.001$  versus control, \*\*  $p < 0.01$ , \*\*\*  $p < 0.001$  versus LPS).

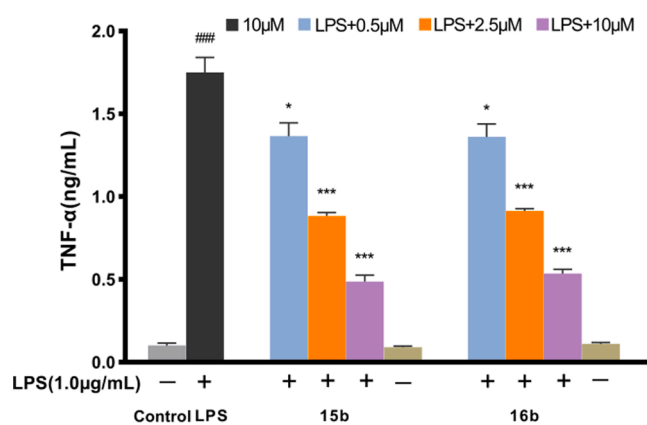


Fig. 9. Effects of compounds **15b** and **16b** on TNF-α release in LPS-stimulated BV-2 cells (n = 3, mean ± SD; ###  $p < 0.001$  versus control, \*  $p < 0.05$ , \*\*\*  $p < 0.001$  versus LPS).

**16b** inhibited the release of NO and TNF-α in LPS-induced BV-2 cells, indicating that they exhibited good anti-neuroinflammatory activities *in vitro* and could be beneficial to the treatment of AD.

#### 2.2.12. *In vitro* blood–brain barrier permeation assay

Penetrating the blood–brain barrier (BBB), followed by reaching the central nervous system (CNS), is crucial to determine the efficacy of drugs and development value as candidate anti-AD drugs. Thus, we

Table 3

Permeability results  $P_e$  ( $\times 10^{-6}$  cm/s) from the PAMPA-BBB assay for selected 4-(aminoalkyl)-1-(2*H*)-phthalazinone derivatives with their predicted penetration into the CNS.

Compd. <sup>a</sup>	$P_e$ ( $\times 10^{-6}$ cm/s) <sup>b</sup>	Prediction
<b>15b</b>	$4.29 \pm 0.32$	CNS +
<b>16b</b>	$10.55 \pm 0.40$	CNS +

<sup>a</sup> Compounds were dissolved in DMSO and diluted with PBS/EtOH (70:30). The final concentration of each compound was 100 µg/mL.

<sup>b</sup> Data are the mean ± SD of three independent experiments.

carried out the parallel artificial membrane permeation assay of the blood–brain barrier (PAMPA-BBB) reported by Di *et al.* to evaluate the BBB permeability of our designed derivatives [54]. Based on the above pharmacological test results, **15b** and **16b** were selected as the representative compounds to assess their permeability. First, the permeability of 11 commercial drugs were detected and compared with the literature value to validate the assay (Supplementary Table S1). A plot of experimental data versus the literature values obtained a good linear correlation [49],  $P_e$  (exp.) =  $0.9163 \times P_e$  (bibl.) - 0.2247 ( $R^2 = 0.9558$ ) (Supplementary Fig. S1). Then, according to the correlation equation and the evaluation conditions established by Di, we defined that compounds with  $P_e$  values higher than  $3.44 \times 10^{-6}$  cm/s could across the BBB. As shown in Table 3, the  $P_e$  values of compounds **15b** and **16b** were  $4.29 \times 10^{-6}$  cm/s and  $10.55 \times 10^{-6}$  cm/s, respectively, which indicated that compounds **15b** and **16b** could penetrate the BBB and reach the CNS. In addition, the longer the methylene linkers of the tested compounds were, the better permeability the compounds exhibited. In summary, these measured results about BBB permeability suggested that this series of compounds may be drugable and of good clinical applicability.

### 3. Conclusion

In summary, our study presented aimed to developing new small molecule ligands endowed with multi-target biological activities against AD. A series of 4-aminoalkyl-1-(2*H*)-phthalazinone derivatives were designed, synthesized and evaluated as multifunctional agents for AD therapy. Overall, *in vitro* assays demonstrated that most of the synthesized compounds, compared with the lead phthalide alkyl tertiary amine derivatives, possessed enhanced inhibition of MAOs, self- and  $\text{Cu}^{2+}$ -induced  $\text{A}\beta_{1-42}$  aggregation and platelet aggregation, almost equivalent antioxidant activities and slightly decreased AChE inhibitory effects, which indicated that this new series of derivatives have more balanced and effective multi-target potencies against AD, consist with our expectations. Among these synthesized derivatives, compound **15b** was

demonstrated as a potent and balanced multi-target candidate for AD. The kinetic analysis and molecular modeling study suggested **15b** was a mixed-type AChE inhibitor ( $IC_{50} = 8.24 \mu\text{M}$ ), and could bind to both CAS and PAS of AChE. In addition, **15b** also exhibited highest inhibition potency towards MAO-B and MAO-A ( $IC_{50} = 0.72 \mu\text{M}$  and  $6.41 \mu\text{M}$  respectively), good inhibition of self- and  $\text{Cu}^{2+}$ -induced  $A\beta_{1-42}$  aggregation, platelet aggregation and neuroinflammation, effective antioxidant activity and neuroprotective potency. Moreover, **15b** manifested the appropriate BBB permeability to enter the brain. Taken together, these outstanding and comprehensive properties qualified compound **15b** as a promising multi-target candidate for AD therapy, worthy of further studies.

## 4. Experimental section

### 4.1. General chemistry

All reagents and solvents, unless otherwise noted, were purchased from commercial sources and used without further purification. The  $^1\text{H}$  NMR and  $^{13}\text{C}$  NMR spectra were recorded in  $\text{CDCl}_3$  or  $\text{DMSO}-d_6$  using TMS as the internal standard on a Varian INOVA spectrometer at  $25^\circ\text{C}$ . Coupling constants are given in Hz. Mass spectra were recorded on Agilent-6210 TOF LC-MS Spectrometer. And melting points were measured on YRT-3 melting-point apparatus (China). The purity of all the target compounds was confirmed through HPLC analysis on a Shimadzu LC-10Avp plus system by a Kromasil C 18 column ( $4.6 \text{ mm} \times 250 \text{ mm}$ ,  $5 \mu\text{m}$ ). The mobile phase was a mixture of methanol and water and the injection volume was  $20 \mu\text{L}$ . Separation was performed under a constant temperature of  $37^\circ\text{C}$  and the effluent was monitored at a UV absorption wavelength of  $254 \text{ nm}$  with a flow rate of  $1.0 \text{ mL/min}$ . In addition, reaction progress was monitored by thin-layer chromatography (TLC) using silica gel GF 254 plates from Qingdao Haiyang Chemical Co. Ltd. (China). The spots were visualized under a UV lamp or in iodine chamber. Column chromatography was performed using silica gel (230–400 mesh) purchased from Qingdao Haiyang Chemical Co. Ltd. (China).

#### 4.1.1. General procedure for the synthesis of $\alpha$ , $\omega$ -diol benzoic acid monoesters (**2a** or **2b**)

A mixture of corresponding  $\alpha,\omega$ -diols **1a** or **1b** (5.0 equiv.) and triethylamine (1.2 equiv.) in THF was stirred at room temperature for 10 min. After that, the reaction mixture was cooled to  $0^\circ\text{C}$ , and then a solution of benzoyl chloride (1.0 equiv.) in THF was added dropwise. The reaction mixture was stirred at  $50^\circ\text{C}$  for an additional 3 h. Upon completion of the reaction, water was added to the mixture and then extracted with ethyl acetate. The combined organic phases were washed with saturated aqueous solution of  $\text{NaHCO}_3$  and brine, dried over anhydrous  $\text{Na}_2\text{SO}_4$ , filtered and evaporated to dryness to afford crude intermediate **2a** or **2b**.

#### 4.1.2. General procedure for the synthesis of benzoyloxyalkyl aldehydes (**3a** or **3b**)

Cyanuric chloride (1.5 equiv.) was dissolved in THF at room temperature. When the solution cooled to about  $-30^\circ\text{C}$ , a solution of DMSO (6 equiv.) in tetrahydrofuran was added slowly and stirred for 30 min. Then to the mixture intermediate **2a** or **2b** (1.0 equiv.) in THF was added and stirred for another 30 min, followed by triethylamine and the reaction mixture stirred at  $-30^\circ\text{C}$  for 20 min. Later, the solution was allowed to warm up to room temperature and kept for 3 h and then concentrated in vacuum. To the residue 5% aqueous HCl was added, extracted with ethyl acetate, washed with saturated aqueous solution of  $\text{NaHCO}_3$  and brine, dried over sodium sulfate and filtered, concentrated under reduced pressure to give the crude compound **3a** or **3b**; yield 85.2% (**3a**) and 90.5% (**3b**).

#### 4.1.3. Synthesis of 3-bromo-5,6-dimethoxyisobenzofuran-1(3H)-one (**5**)

To a solution of 5,6-dimethoxyisobenzofuran-1(3H)-one (**4**) (2 g, 10.30 mmol) and AIBN (100 mg, 0.60 mmol) in dry chlorobenzene (40 mL), under an argon atmosphere and heated to  $85^\circ\text{C}$ , was added NBS (2.02 g, 11.33 mmol) slowly in portions. After the addition, the mixture was kept at  $85^\circ\text{C}$  for 3 h. The mixture was cooled to room temperature, filtered and washed with dry chlorobenzene three times, concentrated under reduced pressure to afford the crude compound **5** as a brown oil; yield 78.2%.

#### 4.1.4. Synthesis of 3-hydroxy-5,6-dimethoxyisobenzofuran-1(3H)-one (**6**)

A mixture of compound **5** (2 g, 7.32 mmol) and  $\text{H}_2\text{O}$  (20 mL) was refluxed for 2 h. After completion of the reaction as indicated by TLC, the white solid crude was filtered from the reaction mixture, washed with aqueous 10% solution of HCl two times, and dried to yield white solid product **6**; yield 65.8%; mp  $173.5 \sim 175.6^\circ\text{C}$ ; (Lit. [55]  $173.0 \sim 176.0^\circ\text{C}$ ).

#### 4.1.5. Synthesis of (5,6-Dimethoxyisobenzofuran-1(3H)-one-3-yl) phosphonic acid diethylester (**7**)

Compound **6** (2.5 g, 11 mmol) and triethyl phosphate (3.65 g, 22 mmol) were dissolved in  $\text{CHCl}_3$  (30 mL), and then  $\text{Py}\cdot\text{HClO}_4$  was added at  $0^\circ\text{C}$ . The resulting mixture stirred at room temperature overnight. After that, to the reaction mixture dichloromethane (30 mL) was added, washed with  $\text{H}_2\text{O}$  ( $4 \times 20 \text{ mL}$ ) and brine ( $2 \times 20 \text{ mL}$ ), dried over sodium sulfate and filtered, concentrated under reduced pressure. The obtained residue was recrystallized from ether to afford the desired compound **7** as a light yellow solid; yield 80.5%; mp  $120.1 \sim 122.3^\circ\text{C}$ ;  $^1\text{H}$  NMR (600 MHz,  $\text{CDCl}_3$ )  $\delta$  7.32 (s, 1H), 7.18 (s, 1H), 5.59 (d,  $J = 10.8 \text{ Hz}$ , 1H), 4.34–4.29 (m, 2H), 4.04–4.02 (m, 1H), 4.00 (s, 3H), 3.96 (s, 3H), 3.88–3.83 (m, 1H), 1.43 (t,  $J = 7.2 \text{ Hz}$ , 3H), 1.11 (t,  $J = 7.2 \text{ Hz}$ , 3H).

#### 4.1.6. General procedure for the synthesis of **8a-b**

To a solution of compound **7** (1 equiv.) and corresponding intermediate **3a** or **3b** (1.2 equiv.) in dichloromethane was added ethanol solution of NaOH (1.2 equiv.). The resulting mixture stirred at room temperature for 2 h, to the mixture was added dichloromethane, washed with  $\text{H}_2\text{O}$  and brine, dried over sodium sulfate, filtered and concentrated under reduced pressure to provide the crude product **8a** or **8b**.

#### 4.1.7. General procedure for the synthesis of **9a-b**

Compound **8a** or **8b** (1 equiv.), dimethylamine hydrochloride (3.0 equiv.) and triethylamine (3.0 equiv.) were dissolved in ethanol and refluxed for 3 h under an argon atmosphere. After the reaction was finished, the solvent was evaporated under reduced pressure. Then  $\text{H}_2\text{O}$  was added to the residue and the mixture was extracted with dichloromethane three times. The combined organic phases were washed with brine, dried over sodium sulfate, filtered and evaporated to dryness to afford the corresponding crude product **9a** or **9b**.

#### 4.1.8. General procedure for the synthesis of **10a-b**

To a mixture of compound **9a** or **9b** (1 equiv.) in  $\text{CH}_3\text{OH}/\text{H}_2\text{O}$  (5:1) was added  $\text{K}_2\text{CO}_3$  (2 equiv.). The mixture was stirred at room temperature for 15 h. The organic solvent was evaporated under vacuum and  $\text{H}_2\text{O}$  was added when TLC verified the disappearance of the precursor. Then, the resulting mixture was extracted with dichloromethane three times. The combined organic phases were washed with brine, dried over sodium sulfate, filtered and concentrated under reduced pressure to give corresponding intermediates **10a** (yield 81.3%) or **10b** (yield 78.6%).

#### 4.1.9. General procedure for the synthesis of **11a-b**

Triethylamine (1.2 equiv.) was added to a solution of intermediate **10a** or **10b** (1.0 eq.) in dichloromethane. The mixture was cooled to  $0\text{--}5^\circ\text{C}$ , followed by adding a solution of benzoyl chloride (1.2 equiv.) in dichloromethane and the resulting mixture continued to stir in the ice bath for 5 min. Later, the solution was allowed to warm up to room

temperature and kept overnight. To the resulting reaction mixture was added H<sub>2</sub>O and extracted with dichloromethane three times. Then the combined organic phases were washed with saturated aqueous solution of NaHCO<sub>3</sub> and brine, dried over anhydrous sodium sulfate and evaporated under reduced pressure to afford the corresponding crude products, which were purified on a silica gel chromatography to obtain compound **11a** or **11b**.

**4.1.9.1. 5-[(2-*N,N*-Dimethylcarbamoyl-4,5-dimethoxy)phenyl]-5-oxo-benzenesulfonic acid pentylester (11a).** Synthesized from compound **10a** via general procedure. Purified by column chromatography (petroleum ether/acetone = 20/1, v/v) to afford intermediate **11a** as a white solid; yield 89.4%; mp 127.5 ~ 128.6 °C; <sup>1</sup>H NMR (400 MHz, CDCl<sub>3</sub>) δ 7.90 (d, *J* = 7.6 Hz, 2H), 7.66 (t, *J* = 7.6 Hz, 1H), 7.56 (t, *J* = 7.6 Hz, 2H), 7.28 (s, 1H), 6.75 (s, 1H), 4.08 (t, *J* = 6.4 Hz, 2H), 3.96 (s, 3H), 3.93 (s, 3H), 3.12 (s, 3H), 2.88 (t, *J* = 7.2 Hz, 2H), 2.75 (s, 3H), 1.76–1.75 (m, 4H).

**4.1.9.2. 7-[(2-*N,N*-dimethylcarbamoyl-4,5-dimethoxy)phenyl]-7-oxo-benzenesulfonic acid heptylester (11b).** Synthesized from compound **10b** via general procedure. Purified by column chromatography (petroleum ether/acetone = 20/1, v/v) to afford intermediate **11b** as a light yellow oil; yield 92.0%; <sup>1</sup>H NMR (400 MHz, CDCl<sub>3</sub>) δ 7.91 (d, *J* = 7.6 Hz, 2H), 7.66 (t, *J* = 7.6 Hz, 1H), 7.56 (t, *J* = 7.6 Hz, 2H), 7.29 (s, 1H), 6.76 (s, 1H), 4.05 (t, *J* = 6.4 Hz, 2H), 3.96 (s, 3H), 3.93 (s, 3H), 3.13 (s, 3H), 2.85 (t, *J* = 7.2 Hz, 2H), 2.76 (s, 3H), 1.70–1.64 (m, 4H), 1.35–1.33 (m, 4H).

#### 4.1.10. General procedure for the synthesis of secondary amines (12a-j)

Compounds **12a-j** (colorless or yellow oil, yield 73.6 ~ 93.8%) were prepared as previously reported by Kumpaty et al. [56].

#### 4.1.11. General procedure for the synthesis of derivatives (13-14)

The derivative **13** or **14** was synthesized in acetonitrile at 50 °C for 5–7 h by the reaction of intermediate **11a** or **11b** (1.0 equiv.) with secondary amines (1.0 equiv.) in presence of potassium carbonate (1.7 equiv.). Then H<sub>2</sub>O was added to the reaction solution to obtain a mixture, which was extracted with ethyl acetate three times. The combined organic phases were washed with water two times and 10% aqueous HCl four times to give a combined acidic water layer, of which the pH was adjusted to 13 with 10% aqueous NaOH. Subsequently, the resulting mixture was extracted with dichloromethane three times, the combined organic phases were washed by brine, dried over anhydrous sodium sulfate, filtered, and concentrated in vacuum to give the crude product which was purified by flash chromatography on silica gel to afford the desired compound **13** or **14**.

**4.1.11.1. 2-[5-(*N*-methyl-*N*-benzylamino)pentanoyl]-4,5-dimethoxy-*N,N*-dimethylbenzamide (13a).** Synthesized from compound **11a** and *N*-benzylmethylamine **12a** via general procedure. Purified by column chromatography (petroleum ether/acetone = 10/1, v/v) to afford intermediate **13a** as a light yellow oil; yield 71.1%; <sup>1</sup>H NMR (400 MHz, CDCl<sub>3</sub>) δ 7.35–7.26 (m, 6H), 6.76 (s, 1H), 3.96 (s, 3H), 3.93 (s, 3H), 3.58 (s, 2H), 3.13 (s, 3H), 2.90 (t, *J* = 7.2 Hz, 2H), 2.76 (s, 3H), 2.49 (t, *J* = 7.2 Hz, 2H), 2.26 (s, 3H), 1.77–1.70 (m, 2H), 1.69–1.63 (m, 2H).

**4.1.11.2. 5-(*N*-methyl-*N*-(2-methoxybenzyl)amino)pentanoyl]-4,5-dimethoxy-*N,N*-dimethylbenzamide (13c).** Synthesized from compound **11a** and *N*-(2-methoxybenzyl)methylamine **12c** via general procedure. Purified by column chromatography (petroleum ether/acetone = 10/1, v/v) to afford intermediate **13c** as a light yellow oil; yield 71.5%; <sup>1</sup>H NMR (400 MHz, CDCl<sub>3</sub>) δ 7.41 (d, *J* = 7.2 Hz, 1H), 7.30 (s, 1H), 7.28 (t, *J* = 7.2 Hz, 1H), 6.95 (t, *J* = 7.2 Hz, 1H), 6.88 (d, *J* = 8.0 Hz, 1H), 6.75 (s, 1H), 3.95 (s, 3H), 3.93 (s, 3H), 3.84 (s, 3H), 3.77 (s, 2H), 3.13 (s, 3H), 2.94 (t, *J* = 7.2 Hz, 2H), 2.76 (s, 3H), 2.63 (t, *J* = 7.2 Hz, 2H), 2.37 (s, 3H), 1.79–1.65 (m, 4H).

**4.1.11.3. 2-[5-(*N*-ethyl-*N*-(2-dimethylaminobenzyl)amino)pentanoyl]-4,5-dimethoxy-*N,N*-dimethyl benzamide (13e).** Synthesized from compound **11a** and *N*-(2-dimethylaminobenzyl)ethylamine **12e** via general procedure. Purified by column chromatography (petroleum ether/acetone = 10/1, v/v) to afford intermediate **13e** as a light yellow oil; yield 62.2%; <sup>1</sup>H NMR (600 MHz, CDCl<sub>3</sub>) δ 7.83 (d, *J* = 7.2 Hz, 1H), 7.36 (t, *J* = 7.2 Hz, 1H), 7.32 (s, 1H), 7.22 (d, *J* = 7.2 Hz, 1H), 7.18 (t, *J* = 7.2 Hz, 1H), 6.74 (s, 1H), 4.26 (s, 2H), 3.98 (s, 3H), 3.93 (s, 3H), 3.12 (s, 2H), 2.99–2.90 (m, 6H), 2.76 (s, 2H), 2.63 (s, 6H), 1.98–1.85 (m, 2H), 1.73–1.69 (m, 2H), 1.36–1.30 (m, 5H).

**4.1.11.4. 2-[5-(*N*-ethyl-*N*-(4-dimethylaminobenzyl)amino)pentanoyl]-4,5-dimethoxy-*N,N*-dimethyl benzamide (13f).** Synthesized from compound **11a** and *N*-(4-dimethylaminobenzyl)ethylamine **12f** via general procedure. Purified by column chromatography (petroleum ether/acetone = 10/1, v/v) to afford intermediate **13f** as a light yellow oil; yield 65.2%; <sup>1</sup>H NMR (600 MHz, CDCl<sub>3</sub>) δ 7.32–7.30 (m, 2H), 7.29 (s, 1H), 6.75 (s, 1H), 6.68 (d, *J* = 8.4 Hz, 2H), 3.97 (s, 3H), 3.96 (s, 2H), 3.93 (s, 3H), 3.13 (s, 3H), 2.96 (t, 2H), 2.92 (s, 6H), 2.84–2.80 (m, 2H), 2.80–2.77 (t, 2H), 2.77 (s, 3H), 1.92–1.82 (m, 2H), 1.74–1.70 (m, 2H), 1.34–1.28 (m, 3H).

**4.1.11.5. 2-(5-morpholinovalleryl)-4,5-dimethoxy-*N,N*-dimethylbenzamide (13i).** Synthesized from compound **11a** and morpholine **12i** via general procedure. Purified by column chromatography (petroleum ether/acetone = 10/1, v/v) to afford intermediate **13i** as a light yellow oil; yield 73.1%; <sup>1</sup>H NMR (600 MHz, CDCl<sub>3</sub>) δ 7.30 (s, 1H), 6.76 (s, 1H), 3.96 (s, 3H), 3.93 (s, 3H), 3.77–3.68 (m, 4H), 3.13 (s, 3H), 2.92 (t, *J* = 7.2 Hz, 2H), 2.76 (s, 3H), 2.51–2.44 (m, 4H), 2.39 (t, *J* = 7.2 Hz, 2H), 1.76–1.73 (m, 2H), 1.60–1.58 (m, 2H).

#### 4.1.12. General procedure for the synthesis of 4-(aminoalkyl)-1(2H)-phthalazinone derivatives 15-16

Compound **13** or **14** and hydrazine hydrate were dissolved in ethanol and refluxed for 8 ~ 10 h under an argon atmosphere. After the reaction checked by TLC was finished, the solvent was evaporated under reduced pressure, and the obtained residue was purified by preparative thin-layer chromatography to produce target compound **15** or **16**.

**4.1.12.1. 4-[4-(*N*-methyl-*N*-benzylamino)butyl]-6,7-dimethoxy-1(2H)-phthalazinone (15a).** Synthesized from compound **13a** via general procedure. Purified by preparative thin-layer chromatography using ethyl acetate/methanol (15:1, v/v) as the eluent to produce compound **15a** as a light yellow oil; yield 61.1%; <sup>1</sup>H NMR (400 MHz, CDCl<sub>3</sub>) δ 10.80 (s, 1H), 7.82 (s, 1H), 7.32–7.24 (m, 5H), 7.08 (s, 1H), 4.05 (s, 3H), 4.01 (s, 3H), 3.55 (s, 2H), 2.92 (t, *J* = 7.2 Hz, 2H), 2.50 (t, *J* = 7.2 Hz, 2H), 2.24 (s, 3H), 1.89–1.81 (m, 2H), 1.75–1.69 (m, 2H). <sup>13</sup>C NMR (150 MHz, CDCl<sub>3</sub>) δ 160.5, 153.7, 152.2, 146.4, 138.1, 129.2 (2C), 128.2 (2C), 127.1, 125.7, 122.7, 106.6, 104.6, 61.9, 56.7, 56.4, 56.2, 41.9, 31.8, 26.7, 25.1. ESI-MS *m/z*: 382.2 [M + H]<sup>+</sup>.

**4.1.12.2. 4-[4-(*N*-ethyl-*N*-benzylamino)butyl]-6,7-dimethoxy-1(2H)-phthalazinone (15b).** Synthesized from compound **13b** via general procedure. Purified by preparative thin-layer chromatography using ethyl acetate/methanol (15:1, v/v) as the eluent to produce compound **15b** as a light yellow oil; yield 62.2%; <sup>1</sup>H NMR (400 MHz, CDCl<sub>3</sub>) δ 11.00 (s, 1H), 7.83 (s, 1H), 7.33–7.19 (m, 5H), 7.06 (s, 1H), 4.05 (s, 3H), 4.00 (s, 3H), 3.62 (s, 2H), 2.89 (t, *J* = 7.2 Hz, 2H), 2.57–2.50 (m, 4H), 1.85–1.77 (m, 2H), 1.69–1.63 (m, 2H), 1.06 (t, *J* = 7.2 Hz, 3H). <sup>13</sup>C NMR (150 MHz, CDCl<sub>3</sub>) δ 160.6, 153.7, 152.3, 146.6, 139.1, 128.9 (2C), 128.1 (2C), 126.8, 125.2, 122.8, 106.6, 104.6, 57.8, 56.5, 56.4, 52.6, 47.2, 31.9, 26.5, 25.3, 11.5. ESI-MS *m/z*: 396.2 [M + H]<sup>+</sup>.

**4.1.12.3. 4-[4-(*N*-methyl-*N*-(2-methoxybenzyl)amino)butyl]-6,7-dimethoxy-1(2H)-phthalazinone (15c).** Synthesized from compound **13c** via

general procedure. Purified by preparative thin-layer chromatography using ethyl acetate/methanol (15:1, v/v) as the eluent to produce compound **15c** as a light yellow oil; yield 61.5%;  $^1\text{H}$  NMR (400 MHz,  $\text{CDCl}_3$ )  $\delta$  10.75 (s, 1H), 7.81 (s, 1H), 7.40 (d,  $J = 7.2$  Hz, 1H), 7.29 (t,  $J = 7.2$  Hz, 1H), 7.10 (s, 1H), 6.94 (t,  $J = 7.2$  Hz, 1H), 6.88 (d,  $J = 8.4$  Hz, 1H), 4.05 (s, 3H), 4.02 (s, 3H), 3.81 (s, 3H), 3.79 (s, 2H), 2.95 (t,  $J = 7.2$  Hz, 2H), 2.69 (t,  $J = 7.2$  Hz, 2H), 2.39 (s, 3H), 1.86–1.69 (m, 4H).  $^{13}\text{C}$  NMR (150 MHz,  $\text{CDCl}_3$ )  $\delta$  160.5, 157.9, 153.7, 152.3, 146.3, 131.6 (2C), 129.3, 125.1, 122.6, 120.5, 110.5, 106.5, 104.6, 56.5, 56.4, 56.3, 55.3, 54.6, 41.3, 31.6, 25.9, 24.9. ESI-MS  $m/z$ : 412.2  $[\text{M} + \text{H}]^+$ .

**4.1.12.4. 4-[4-(*N*-ethyl-*N*-(2-methoxybenzyl)amino)butyl]-6,7-dimethoxy-1(2*H*)-phthalazinone (**15d**).** Synthesized from compound **13d** via general procedure. Purified by preparative thin-layer chromatography using ethyl acetate/methanol (15:1, v/v) as the eluent to produce compound **15d** as a light yellow oil; yield 59.5%;  $^1\text{H}$  NMR (400 MHz,  $\text{CDCl}_3$ )  $\delta$  10.89 (s, 1H), 7.82 (s, 1H), 7.48 (d,  $J = 6.8$  Hz, 1H), 7.26 (t,  $J = 6.8$  Hz, 1H), 7.08 (s, 1H), 6.93 (t,  $J = 7.2$  Hz, 1H), 6.86 (d,  $J = 8.0$  Hz, 1H), 4.05 (s, 3H), 4.01 (s, 3H), 3.81 (s, 2H), 3.80 (s, 3H), 2.92 (t,  $J = 7.2$  Hz, 2H), 2.79–2.61 (m, 4H), 1.92–1.69 (m, 4H), 1.25–1.10 (m, 3H).  $^{13}\text{C}$  NMR (150 MHz,  $\text{CDCl}_3$ )  $\delta$  160.3, 157.8, 153.8, 152.3, 146.3, 131.1 (2C), 128.9, 125.1, 122.7, 120.5, 110.4, 106.6, 104.6, 56.4, 56.3, 55.3, 52.5, 50.8, 47.4, 31.7, 25.7, 25.0, 10.7. ESI-MS  $m/z$ : 426.2  $[\text{M} + \text{H}]^+$ .

**4.1.12.5. 4-[4-(*N*-ethyl-*N*-(2-dimethylaminobenzyl)amino)butyl]-6,7-dimethoxy-1(2*H*)-phthalazinone (**15e**).** Synthesized from compound **13e** via general procedure. Purified by preparative thin-layer chromatography using ethyl acetate/methanol (15:1, v/v) as the eluent to produce compound **15e** as a light yellow oil; yield 52.2%;  $^1\text{H}$  NMR (400 MHz,  $\text{CDCl}_3$ )  $\delta$  10.87 (s, 1H), 7.82–7.75 (m, 2H), 7.29 (t,  $J = 7.2$  Hz, 1H), 7.17–7.08 (m, 3H), 4.06 (s, 2H), 4.05 (s, 6H), 2.94 (t,  $J = 7.2$  Hz, 2H), 2.90–2.78 (m, 2H), 2.65 (s, 6H), 1.95–1.78 (m, 3H), 1.32–1.15 (m, 4H).  $^{13}\text{C}$  NMR (150 MHz,  $\text{CDCl}_3$ )  $\delta$  160.3, 153.9, 153.6, 152.4, 146.0, 131.3, 129.2, 125.1, 124.2, 122.6, 119.8, 106.6, 104.6, 56.4, 52.3, 51.3, 47.1, 45.1, 31.4, 29.6, 29.3, 24.9, 24.6, 9.7. ESI-MS  $m/z$ : 438.8  $[\text{M} + \text{H}]^+$ .

**4.1.12.6. 4-[4-(*N*-ethyl-*N*-(4-dimethylaminobenzyl)amino)butyl]-6,7-dimethoxy-1(2*H*)-phthalazinone (**15f**).** Synthesized from compound **13f** via general procedure. Purified by preparative thin-layer chromatography using ethyl acetate/methanol (15:1, v/v) as the eluent to produce compound **15f** as a light yellow oil; yield 52.2%;  $^1\text{H}$  NMR (400 MHz,  $\text{CDCl}_3$ )  $\delta$  10.75 (s, 1H), 7.81 (s, 1H), 7.23 (d,  $J = 8.4$  Hz, 2H), 7.08 (s, 1H), 6.66 (d,  $J = 8.4$  Hz, 2H), 4.05 (s, 3H), 4.03 (s, 3H), 3.74 (s, 2H), 2.93 (s, 6H), 2.92 (t,  $J = 7.2$  Hz, 2H), 2.80–2.61 (m, 4H), 1.86–1.79 (m, 4H), 1.22–1.18 (m, 3H).  $^{13}\text{C}$  NMR (150 MHz,  $\text{CDCl}_3$ )  $\delta$  160.4, 153.7, 152.3, 150.2, 146.1, 130.7 (2C), 128.1, 125.1, 122.6, 112.2 (2C), 106.5, 104.5, 56.5, 56.4, 56.3, 51.6, 46.6, 40.4 (2C), 31.5, 25.2, 24.8, 10.4. ESI-MS  $m/z$ : 439.1  $[\text{M} + \text{H}]^+$ .

**4.1.12.7. 4-(4-piperidylbutyl)-6,7-dimethoxy-1(2*H*)-phthalazinone (**15g**).** Synthesized from compound **13g** via general procedure. Purified by preparative thin-layer chromatography using ethyl acetate/methanol (15:1, v/v) as the eluent to produce compound **15g** as a white solid; mp 83.1 ~ 84.1 °C; yield 52.4%;  $^1\text{H}$  NMR (400 MHz,  $\text{CDCl}_3$ )  $\delta$  11.19 (s, 1H), 7.79 (s, 1H), 7.08 (s, 1H), 4.06 (s, 3H), 4.05 (s, 3H), 2.98–2.92 (m, 2H), 2.78–2.67 (m, 6H), 2.00–1.84 (m, 8H), 1.71–1.55 (m, 2H).  $^{13}\text{C}$  NMR (150 MHz,  $\text{DMSO}-d_6$ )  $\delta$  159.5, 153.6, 152.3, 145.5, 124.8, 122.6, 106.2, 105.9, 57.7, 56.4, 56.2, 53.7 (2C), 31.3, 25.2, 25.1, 24.8 (2C), 23.6. ESI-MS  $m/z$ : 346.2  $[\text{M} + \text{H}]^+$ .

**4.1.12.8. 4-(4-Diethylaminobutyl)-6,7-dimethoxy-1(2*H*)-phthalazinone (**15h**).** Synthesized from compound **13h** via general procedure. Purified by preparative thin-layer chromatography using ethyl acetate/methanol (15:1, v/v) as the eluent to produce compound **15h** as a white solid; mp 59.4 ~ 60.5 °C; yield 51.5%;  $^1\text{H}$  NMR (400 MHz,  $\text{DMSO}-d_6$ )  $\delta$

12.37 (s, 1H), 7.62 (s, 1H), 7.28 (s, 1H), 3.99 (s, 3H), 3.94 (s, 3H), 3.12–3.01 (m, 6H), 2.99–2.94 (m, 2H), 1.82–1.72 (m, 4H), 1.23–1.19 (m, 6H).  $^{13}\text{C}$  NMR (150 MHz,  $\text{DMSO}-d_6$ )  $\delta$  159.5, 153.7, 152.4, 145.2, 124.8, 122.6, 106.3, 106.0, 56.6, 56.3, 50.9, 46.5 (2C), 31.0, 24.6, 23.3, 9.0 (2C). ESI-MS  $m/z$ : 334.2  $[\text{M} + \text{H}]^+$ .

**4.1.12.9. 4-(4-morpholinylbutyl)-6,7-dimethoxy-1(2*H*)-phthalazinone (**15i**).** Synthesized from compound **13i** via general procedure. Purified by preparative thin-layer chromatography using ethyl acetate/methanol (15:1, v/v) as the eluent to produce compound **15i** as a white solid; mp 192.8 ~ 194.1 °C; yield 50.1%;  $^1\text{H}$  NMR (400 MHz,  $\text{CDCl}_3$ )  $\delta$  10.74 (s, 1H), 7.81 (s, 1H), 7.08 (s, 1H), 4.05 (s, 3H), 4.04 (s, 3H), 3.81–3.75 (m, 4H), 2.95 (t,  $J = 7.2$  Hz, 2H), 2.57–2.52 (m, 6H), 1.89–1.77 (m, 2H), 1.69–1.61 (m, 2H).  $^{13}\text{C}$  NMR (150 MHz,  $\text{CDCl}_3$ )  $\delta$  160.4, 153.7, 152.3, 146.2, 125.1, 122.8, 106.6, 104.6, 66.7, 58.5, 56.5, 56.4, 56.3, 56.2, 53.6, 31.8, 26.0, 25.1. ESI-MS  $m/z$ : 348.3  $[\text{M} + \text{H}]^+$ .

**4.1.12.10. 4-[4-(4-Methylpiperazin-1-yl)butyl]-6,7-dimethoxy-1(2*H*)-phthalazinone (**15j**).** Synthesized from compound **14j** via general procedure. Purified by preparative thin-layer chromatography using ethyl acetate/methanol (15:1, v/v) as the eluent to produce compound **15j** as a white solid; mp 108.7 ~ 109.9 °C; yield 51.2%;  $^1\text{H}$  NMR (400 MHz,  $\text{CDCl}_3$ )  $\delta$  11.15 (s, 1H), 7.81 (s, 1H), 7.08 (s, 1H), 4.05 (s, 3H), 4.02 (s, 3H), 2.93 (t,  $J = 7.6$  Hz, 2H), 2.72–2.50 (m, 8H), 2.48 (t,  $J = 7.6$  Hz, 2H), 2.34 (s, 3H), 1.86–1.79 (m, 2H), 1.70–1.66 (m, 2H).  $^{13}\text{C}$  NMR (150 MHz,  $\text{CDCl}_3$ )  $\delta$  160.3, 153.7, 152.3, 146.2, 125.1, 122.8, 106.6, 104.5, 58.0, 56.4, 56.3, 54.6 (2C), 52.7 (2C), 45.7, 31.8, 26.3, 25.2. ESI-MS  $m/z$ : 361.2  $[\text{M} + \text{H}]^+$ .

**4.1.12.11. 4-[6-(*N*-methyl-*N*-benzylamino)hexyl]-6,7-dimethoxy-1(2*H*)-phthalazinone (**16a**).** Synthesized from compound **14a** via general procedure. Purified by preparative thin-layer chromatography using ethyl acetate/methanol (15:1, v/v) as the eluent to produce compound **16a** as a light yellow oil; yield 61.8%;  $^1\text{H}$  NMR (600 MHz,  $\text{CDCl}_3$ )  $\delta$  10.75 (s, 1H), 7.83 (s, 1H), 7.32–7.25 (m, 5H), 7.09 (s, 1H), 4.05 (s, 3H), 4.04 (s, 3H), 3.52 (s, 2H), 2.90 (t,  $J = 7.2$  Hz, 2H), 2.41 (t,  $J = 7.2$  Hz, 2H), 2.21 (s, 3H), 1.82–1.77 (m, 2H), 1.60–1.55 (m, 2H), 1.48–1.39 (m, 4H).  $^{13}\text{C}$  NMR (150 MHz,  $\text{CDCl}_3$ )  $\delta$  160.4, 153.8, 152.3, 146.7, 138.1, 129.2 (2C), 128.2 (2C), 127.1, 125.2, 122.9, 106.7, 104.7, 62.2, 57.2, 56.5, 56.3, 42.0, 32.1, 29.3, 27.6, 27.2, 27.1. ESI-MS  $m/z$ : 410.2  $[\text{M} + \text{H}]^+$ .

**4.1.12.12. 4-[6-(*N*-ethyl-*N*-benzylamino)hexyl]-6,7-dimethoxy-1(2*H*)-phthalazinone (**16b**).** Synthesized from compound **14b** via general procedure. Purified by preparative thin-layer chromatography using ethyl acetate/methanol (15:1, v/v) as the eluent to produce compound **16b** as a light yellow oil; yield 60.2%;  $^1\text{H}$  NMR (400 MHz,  $\text{CDCl}_3$ )  $\delta$  10.77 (s, 1H), 7.83 (s, 1H), 7.35–7.21 (m, 5H), 7.08 (s, 1H), 4.05 (s, 3H), 4.03 (s, 3H), 3.60 (s, 2H), 2.89 (t,  $J = 7.6$  Hz, 2H), 2.54 (q,  $J = 7.2$  Hz, 2H), 2.46 (t,  $J = 7.2$  Hz, 2H), 1.82–1.74 (m, 2H), 1.57–1.51 (m, 2H), 1.47–1.28 (m, 4H), 1.06 (t,  $J = 7.2$  Hz, 3H).  $^{13}\text{C}$  NMR (150 MHz,  $\text{CDCl}_3$ )  $\delta$  160.2, 153.7, 152.3, 146.7, 138.2, 128.9 (2C), 128.1 (2C), 126.8, 125.1, 122.8, 106.7, 104.7, 57.8, 56.4, 56.2, 52.8, 47.1, 32.0, 29.2, 27.5, 27.1, 26.6, 11.3. ESI-MS  $m/z$ : 424.3  $[\text{M} + \text{H}]^+$ .

**4.1.12.13. 4-[6-(*N*-methyl-*N*-(2-methoxybenzyl)amino)hexyl]-6,7-dimethoxy-1(2*H*)-phthalazinone (**16c**).** Synthesized from compound **14c** via general procedure. Purified by preparative thin-layer chromatography using ethyl acetate/methanol (15:1, v/v) as the eluent to produce compound **16c** as a light yellow oil; yield 59.5%;  $^1\text{H}$  NMR (400 MHz,  $\text{CDCl}_3$ )  $\delta$  10.86 (s, 1H), 7.82 (s, 1H), 7.40 (d,  $J = 7.2$  Hz, 1H), 7.28 (t,  $J = 7.2$  Hz, 1H), 7.10 (s, 1H), 6.95 (t,  $J = 7.2$  Hz, 1H), 6.88 (d,  $J = 8.0$  Hz, 1H), 4.05 (s, 3H), 4.00 (s, 3H), 3.83 (s, 3H), 3.76 (s, 2H), 2.90 (t,  $J = 7.2$  Hz, 2H), 2.61–2.55 (m, 2H), 2.37 (s, 3H), 1.86–1.78 (m, 2H), 1.77–1.62 (m, 2H), 1.55–1.36 (m, 4H).  $^{13}\text{C}$  NMR (150 MHz,  $\text{CDCl}_3$ )  $\delta$  160.3, 157.9, 153.8, 152.3, 146.6, 131.5 (2C), 129.3, 125.2, 122.8, 120.5, 110.5,

106.7, 104.7, 56.9, 56.5, 56.3, 55.4, 54.6, 41.3, 32.0, 29.0, 27.3, 27.0, 26.1. ESI-MS  $m/z$ : 439.8 [M + H]<sup>+</sup>.

4.1.12.14. 4-[6-(*N*-ethyl-*N*-(2-methoxybenzyl)amino)hexyl]-6,7-dimethoxy-1(2*H*)-phthalazinone (**16d**). Synthesized from compound **14d** via general procedure. Purified by preparative thin-layer chromatography using ethyl acetate/methanol (15:1, v/v) as the eluent to produce compound **16d** as a light yellow oil; yield 59.8%; <sup>1</sup>H NMR (400 MHz, CDCl<sub>3</sub>) δ 10.85 (s, 1H), 7.83 (s, 1H), 7.55 (d, *J* = 7.6 Hz, 1H), 7.28 (t, *J* = 7.6 Hz, 1H), 7.09 (s, 1H), 6.98 (t, *J* = 7.2 Hz, 1H), 6.89 (d, *J* = 8.4 Hz, 1H), 4.05 (s, 3H), 4.02 (s, 3H), 3.95 (s, 2H), 3.84 (s, 3H), 2.90 (t, *J* = 7.2 Hz, 2H), 2.87–2.79 (m, 2H), 2.78–2.71 (m, 2H), 1.82–1.73 (m, 4H), 1.47–1.38 (m, 4H), 1.25–1.20 (m, 3H). <sup>13</sup>C NMR (150 MHz, CDCl<sub>3</sub>) δ 160.3, 157.8, 153.8, 152.3, 146.5, 131.8 (2C), 128.9, 125.2, 122.7, 120.8, 110.5, 106.6, 104.7, 56.4, 56.3, 55.4, 52.3, 50.5, 47.1, 31.9, 28.9, 27.2, 27.0, 25.0, 10.2. ESI-MS  $m/z$ : 454.2 [M + H]<sup>+</sup>.

4.1.12.15. 4-[6-(*N*-ethyl-*N*-(2-dimethylaminobenzyl)amino)hexyl]-6,7-dimethoxy-1(2*H*)-phthalazinone (**16e**). Synthesized from compound **14e** via general procedure. Purified by preparative thin-layer chromatography using ethyl acetate/methanol (15:1, v/v) as the eluent to produce compound **16e** as a light yellow oil; yield 52.8%; <sup>1</sup>H NMR (400 MHz, CDCl<sub>3</sub>) δ 10.49 (s, 1H), 7.88 (d, *J* = 7.2 Hz, 1H), 7.81 (s, 1H), 7.34 (t, *J* = 7.2 Hz, 1H), 7.23–7.14 (m, 2H), 7.09 (s, 1H), 4.28 (s, 2H), 4.07 (s, 3H), 4.05 (s, 3H), 3.08–2.87 (m, 6H), 2.65 (s, 6H), 1.83–1.45 (m, 4H), 1.44–1.28 (m, 7H). <sup>13</sup>C NMR (150 MHz, CDCl<sub>3</sub>) δ 160.1, 153.9, 153.6, 152.4, 146.3, 132.0 (2C), 130.4, 125.2, 125.0, 122.7, 120.4, 106.7, 104.7, 56.5, 51.8, 50.6, 46.7, 45.6 (2C), 31.7, 29.7, 28.7, 26.9, 26.7, 23.6, 8.8. ESI-MS  $m/z$ : 467.3 [M + H]<sup>+</sup>.

4.1.12.16. 4-[6-(*N*-ethyl-*N*-(4-dimethylaminobenzyl)amino)hexyl]-6,7-dimethoxy-1(2*H*)-phthalazinone (**16f**). Synthesized from compound **14f** via general procedure. Purified by preparative thin-layer chromatography using ethyl acetate/methanol (15:1, v/v) as the eluent to produce compound **16f** as a light yellow oil; yield 52.2%; <sup>1</sup>H NMR (400 MHz, CDCl<sub>3</sub>) δ 10.50 (s, 1H), 7.82 (s, 1H), 7.27 (d, *J* = 8.4 Hz, 2H), 7.09 (s, 1H), 6.69 (d, *J* = 8.4 Hz, 2H), 4.06 (s, 3H), 4.05 (s, 3H), 3.78 (s, 2H), 2.98 (s, 6H), 2.89 (t, *J* = 7.2 Hz, 2H), 2.80–2.71 (m, 2H), 2.69–2.61 (m, 2H), 1.81–1.67 (m, 4H), 1.46–1.38 (m, 4H), 1.25–1.22 (m, 3H). <sup>13</sup>C NMR (150 MHz, CDCl<sub>3</sub>) δ 160.0, 153.7, 152.3, 150.3, 146.5, 130.9 (2C), 128.1, 125.1, 122.7, 112.3 (2C), 106.6, 104.7, 56.4, 56.3, 51.7, 46.4, 40.4 (2C), 31.8, 29.6, 28.9, 27.1, 26.9, 25.1, 10.2. ESI-MS  $m/z$ : 467.3 [M + H]<sup>+</sup>.

#### 4.1.13. Synthesis of 5,6-dimethoxyphthalic anhydride (**18**)

In a 10 mL round bottom flask, 4,5-dimethoxyphthalic acid (**17**) (600 mg, 2.65 mmol) and acetic anhydride (1 mL, 10.61 mmol) were dissolved in tetrahydrofuran (3 mL) and refluxed for 5 h. To remove tetrahydrofuran and acetic anhydride of the mixture, it was evaporated under reduced pressure. Then petroleum ether (5 mL) was added to the residue, refluxed for 5 min and filtered while hot. The resulting residue was washed with an appropriate amount of petroleum ether, and dried in vacuum to obtain compound **18** as a white solid; yield 94.8%; mp 178.2 ~ 179.6 °C. (Lit. [57] 179 ~ 181 °C)

#### 4.1.14. Synthesis of (*E/Z*)-2-(5,6-dimethoxyisobenzofuran-1-one-3-ylidene) ethyl acetate (**19**)

To a solution of compound **18** (168 mg, 0.48 mmol) in toluene (2 mL) was added ethyl 2-(triphenylphosphinidene)acetate (100 mg, 0.48 mmol) prepared as the literature reported [38] and refluxed for 3 h. Upon completion and cooling to room temperature, the solvent was evaporated under reduced pressure, and the obtained residue was purified by column chromatography to afford intermediate **19** as a white solid; yield 89%; mp 155.1 ~ 158.0 °C (Lit. [58] (*E*)-2-(5,6-dimethoxyisobenzofuran-3-one-1-ylidene) ethyl acetate 168 ~ 170 °C; (*Z*)-2-(5,6-

dimethoxyisobenzofuran-3-one-1-ylidene) ethyl acetate 212 ~ 214 °C).

#### 4.1.15. Synthesis of 2-(6,7-dimethoxy-1(2*H*)-phthalazinone-4-yl)ethyl acetate (**20**)

(*E/Z*)-2-(5,6-dimethoxyisobenzofuran-1-one-3-ylidene) ethyl acetate (**19**) (360 mg, 1.3 mmol) and hydrazine hydrate (0.16 mL, 2.6 mmol) were resolved in ethanol (3 mL) and refluxed for 3 h. After the reaction was finished, the solvent was evaporated under reduced pressure, and the obtained residue was purified by column chromatography to afford intermediate **20** as a white solid; yield 83%; mp 183.1 ~ 186.0 °C; <sup>1</sup>H NMR (400 MHz, CDCl<sub>3</sub>) δ 10.68 (s, 1H), 7.82 (s, 1H), 7.10 (s, 1H), 4.19 (q, *J* = 7.2 Hz, 2H), 4.05 (s, 3H), 4.02 (s, 3H), 3.94 (s, 2H), 1.28–1.22 (m, 3H).

#### 4.1.16. Synthesis of 4-(2-hydroxyethyl)-6,7-dimethoxy-1(2*H*)-phthalazinone (**21**)

To a solution of intermediate **20** (180 mg, 0.65 mmol) in ethanol (2 mL) and tetrahydrofuran (0.5 mL) was added sodium borohydride (100 mg, 2.6 mmol) and lithium chloride (112 mg, 2.6 mmol) at 0–5 °C, stirred and kept for 30 min. The mixture was warmed up to room temperature and stirred overnight. Then, the pH of the reaction mixture was adjusted to 4 with aqueous 10% solution of HCl, stirred at room temperature for 30 min and filtered to give the residue, which was recrystallized to afford product **21** as a white solid; yield 80.1%; mp > 220 °C.

#### 4.1.17. Synthesis of 4-(2-chloroethyl)-6,7-dimethoxy-1(2*H*)-phthalazinone (**22**)

Thionyl chloride (0.03 mL, 0.48 mmol) was added to the solution of compound **21** in *N,N*-dimethylformamide (1 drop) and chloroform (2 mL) and refluxed for 10 h. After the reaction was finished, the solvent of the mixture was evaporated in vacuum to give the crude product, which was then recrystallized with ethanol to yield compound **22** as a light yellow solid; yield 89.2%; mp > 220 °C; <sup>1</sup>H NMR (600 MHz, DMSO-*d*<sub>6</sub>) δ 12.45 (s, 1H), 7.62 (s, 1H), 7.30 (s, 1H), 4.04 (t, *J* = 6.6 Hz, 2H), 3.99 (s, 3H), 3.94 (s, 3H), 3.24 (t, *J* = 6.0 Hz, 2H).

#### 4.1.18. General procedure for the synthesis of 4-(aminoalkyl)-1(2*H*)-phthalazinone derivatives (**23a** or **23c**)

The target compound **23a** or **23c** was synthesized in acetonitrile under reflux condition for 10 h by the reaction of compound **22** (1.0 equiv.) with the corresponding secondary amine **12a** or **12c** (1.5 equiv.) in presence of potassium carbonate (1.5 equiv.) and a catalytic amount of tetrabutylammonium bromide (TBAB). After the reaction was finished, the solvent was evaporated under reduced pressure. Then H<sub>2</sub>O was added to the residue and the mixture was extracted with dichloromethane. The combined organic phases were washed with brine, dried over sodium sulfate, filtered and concentrated under reduced pressure to obtain the crude product, which was then purified by preparative thin-layer chromatography to yield compound **23a** or **23c**.

4.1.18.1. 4-[2-(*N*-methyl-*N*-benzylamino)ethyl]-6,7-dimethoxy-1(2*H*)-phthalazinone (**23a**). Synthesized from compound **22** and *N*-benzylmethylamine (**12a**) via general procedure. Purified by preparative thin-layer chromatography using ethyl acetate/methanol (15:1, v/v) as the eluent to produce compound **23a** as a light yellow oil; yield 62.1%; <sup>1</sup>H NMR (400 MHz, CDCl<sub>3</sub>) δ 10.39 (s, 1H), 7.79 (s, 1H), 7.30–7.26 (m, 5H), 7.04 (s, 1H), 4.04 (s, 3H), 3.91 (s, 3H), 3.66 (s, 2H), 3.15 (t, *J* = 7.2 Hz, 2H), 2.88 (t, *J* = 7.2 Hz, 2H), 2.43 (s, 3H). ESI-MS  $m/z$ : 354.2 [M + H]<sup>+</sup>.

4.1.18.2. 4-[2-(*N*-methyl-*N*-(2-methoxybenzyl)amino)ethyl]-6,7-dimethoxy-1(2*H*)-phthalazinone (**23c**). Synthesized from compound **22** and *N*-benzylmethylamine (**12c**) via general procedure. Purified by preparative thin-layer chromatography using ethyl acetate/methanol (15:1, v/v) as the eluent to produce compound **23c** as a light yellow oil; yield 63.2%; <sup>1</sup>H NMR (400 MHz, CDCl<sub>3</sub>) δ 11.25 (s, 1H), 7.81 (s, 1H),

7.33–7.23 (m, 2H), 7.16 (s, 1H), 6.92–6.85 (m, 2H), 4.05 (s, 3H), 3.95 (s, 3H), 3.82 (s, 3H), 3.74 (s, 2H), 3.25 (t,  $J = 7.6$  Hz, 2H), 2.96 (t,  $J = 7.6$  Hz, 2H), 2.46 (s, 3H).  $^{13}\text{C}$  NMR (150 MHz,  $\text{CDCl}_3$ )  $\delta$  160.5, 157.8, 153.9, 152.4, 145.2, 131.1 (2C), 128.8, 125.2, 122.7, 120.4, 110.5, 106.6, 104.9, 56.5, 56.4, 55.6, 55.4, 55.2, 42.3, 30.3. ESI-MS  $m/z$ : 383.8 [M + H] $^+$ .

## 4.2. Biological evaluation

### 4.2.1. Inhibition experiments of AChE and BuChE

The inhibitory potencies of synthesized compounds on AChE and BuChE were evaluated by the modified Ellman's method [41]. Purified AChE derived from *Electrophorus electricus* (Sigma-Aldrich Co.) and BuChE from rat serum. For the determination of AChE inhibition assay, thioacetylcholine iodide (1 mmol/L, 30  $\mu\text{L}$ ), phosphate-buffered solution (0.1 mmol/L, pH = 8.0, 40  $\mu\text{L}$ ), different concentrations of the tested compounds solution (20  $\mu\text{L}$ , DMSO content <1%) and EeAChE (0.05 U/mL, 10  $\mu\text{L}$ ) were added to the 96-well plate. After shaking for 1 min, incubation for 15 min at 37 °C, then 5,5'-dithiobis-2-nitrobenzoic acid (DTNB, 0.2%, 30  $\mu\text{L}$ ) (J&K Scientific) was added to this mixed solution. The absorbance (OD value) of each well was measured at 412 nm with a Varioskan Flash Multimode Reader (Thermo Scientific). With regard to the BuChE inhibition assay, almost the same method as above was used excepting the differences that butyrylthiocholine iodide (1 mmol/L, 30  $\mu\text{L}$ ) as a substrate, a phosphate-buffered solution (0.1 mmol/L, pH = 7.4) and 25% rat serum supernatant (10  $\mu\text{L}$ ) were used in this assay, and the change in absorbance of each well was measured at 405 nm. In addition, the  $\text{IC}_{50}$  values represented the concentration of inhibitor that produced 50% enzyme activity inhibition. donepezil and Tacrine were used as the positive controls and the results obtained were the average values after performing at least three parallel experiments, expressed as mean  $\pm$  SD.

### 4.2.2. Kinetic study for the inhibition of AChE

The kinetic characterization of the compound for the inhibition of AChE was carried out according to the reported method [42]. To the solution containing phosphate-buffered solution (20  $\mu\text{L}$ , pH = 8.0), EeAChE (0.5 U/mL, 10  $\mu\text{L}$ ), DTNB (30  $\mu\text{L}$ , 0.2%) in 96-well plate was added three different concentrations of tested compounds. After shaking and mixing, the mixed solution was incubated at 37 °C for 15 min, followed by the addition of substrate (ATCh) in different concentrations, and then the OD values were measured and recorded at a wavelength of 412 nm. The parallel control experiments was performed without inhibitor. The resulting graph was analyzed by a weighted least square analysis. Furthermore, the slopes of Lineweaver-Burk curves were plotted against the concentrations of **15b** in a weighted analysis to obtain a linear graph and the intercept on the negative x-axis was the  $K_i$  for the inhibition of AChE.

### 4.2.3. Molecular modeling study

The crystal structure of TcAChE complex with donepezil (PDB: 1EVE) was used to study the molecular docking between compound **15b** and AChE. First, deleting the ligand donepezil to obtain the receptor TcAChE required for the docking. Then, the visualization software Autodock Tools (ADT, version 1.5.6) was used for the setting of docking parameters as well as performing the pretreatment of protein and small molecular, which included two aspects: (1) Adding polar hydrogen to the amino acid residues of the protein, and loading Gasteiger charges on each atom of the protein molecular. (2) Charging the small molecular, calculating and setting freely rotating keys. In addition, the obtained protein structure was calculated, using AUTOGRID, to obtain the atomic affinity grid maps for each atom type in the ligand, which included desolvation and electrostatics. All the maps were calculated with 0.375 Å spacing between grid points., and the grid point was placed at the bottom of the enzyme activity (coordinates: x = 2.023, y = 63.295, z = 67.062). The dimensions of the active site box were set at 60  $\times$  60  $\times$  60

Å. The AUTODOCK4.2 program package was used for molecular docking experiments, and the docking calculation was performed by 100 runs using the Lamarckian genetic algorithm (LGA) of the AUTODOCK. Apart from the mentioned parameters above, others were as defaulted. Furthermore, a cluster analysis of docking results was carried out using a root mean square (RMS) tolerance of 1.0, followed by recording and analyzing the optimal cluster docking results and comprehensive selection. Graphic manipulations and visualizations were done by Autodock Tools or Discovery Studio 2.5 software.

### 4.2.4. In vitro inhibition of MAO [59]

The MAO inhibition assay were carried out using the recombinant human MAO-A and MAO-B purchased from commercial sources (Sigma Co.), pre-aliquoted and stored at  $-80$  °C. Kynurenamine was used as the substrate of MAO, since kynuramine could be oxidized by monoamine oxidase (MAO) to produce 4-hydroxyquinoline, which could further produce fluorescence under alkaline conditions. Thus, the inhibitory potency of the tested compounds towards MAO was measured by detecting its fluorescence value. First, the tested compounds were dissolved with DMSO and diluted with phosphate buffer (100 mM, pH = 7.40, containing 20.2 mM KCl) before use. Then, to the reaction plate was added a final volume of 500  $\mu\text{L}$  containing different concentrations of tested compounds (0–100  $\mu\text{M}$ , 100  $\mu\text{L}$ ), MAO-A solution (12.5  $\mu\text{g}/\text{mL}$ , 300  $\mu\text{L}$ ) and kynuramine solution (225  $\mu\text{M}$ , 100  $\mu\text{L}$ ), with the final concentrations of MAO-A and kynuramine being 7.5  $\mu\text{g}/\text{mL}$  and 45  $\mu\text{M}$ , respectively, and the DMSO content being less than 4%. The obtained mixed solution was incubated for 30 min at 37 °C, then quenched by NaOH solution (2 mol/L, 400  $\mu\text{L}$ ) and distilled water (1000  $\mu\text{L}$ ), followed by centrifuging for 10 min at 16,000 g. After that, the supernatant was extracted and measured the fluorescence intensity using a Varioskan Flash Multimode Reader at excitation and emission wavelengths of 310 nm and 400 nm, respectively.  $\text{IC}_{50}$  values were obtained with excitation wavelength sigmoidal dose–response curves (graphs of the initial rate of kynuramine oxidation versus the logarithm of inhibitor concentration) using GraphPad Prism software and expressed as mean  $\pm$  SD. The drawing of sigmoidal curve required selecting at least six different concentrations of compounds with three orders of magnitude. Each group of experiments were performed independently and repeated for at least three times. In addition, the measurement method of inhibitor activities against MAO-B for tested compounds was almost the same as that against MAO-A, excepting that the concentration of kynuramine added was changed to 150  $\mu\text{M}$ .

### 4.2.5. Molecular modeling study of MAO

The crystal structure of hMAO-A (PDB: 2Z5X) and hMAO-B (PDB: 2V60) were used to study the molecular docking with tested compound **15b** [60]. After performing a series of pretreatments including the removal of the original ligand and water molecular and the addition of polar hydrogen onto both protein and coenzyme factor, AUTODOCK 4.2 program was used to perform the docking studies. Furthermore, each group of docking experiment was calculated by Lamarck Genetic Algorithm (LGA) for 100 times. Finally, a cluster analysis was performed based on the docking results, with a root mean square (RMS) tolerance of 1.0. Noteworthy, the lowest docking-energy conformation of the highest populated cluster was comprehensively selected for the result analysis. Graphic manipulations and visualizations were performed by using Autodock Tools or Discovery Studio 2.5 software.

### 4.2.6. Inhibition of self-induced $A\beta_{1-42}$ aggregation

Thioflavin-T assay was used to measure the inhibitory potencies of tested compounds towards self-induced  $A\beta_{1-42}$  aggregation [61,62]. The commercial  $A\beta_{1-42}$  trifluoroacetate was first dissolved in hexafluoroisopropanol (TFIP) and incubated at room temperature for 24 h. Then, the solvent was evaporated under reduced pressure, the residue was further dissolved in DMSO to obtain the  $A\beta_{1-42}$  solution and stored at  $-80$  °C, and the frozen stock solution above was diluted by potassium

phosphate buffer (50 mM, pH = 7.4) to be at the concentration of 50  $\mu$ M before use. To a 96-well plate was added three different samples including the mixture of  $A\beta_{1-42}$  solution (50  $\mu$ M, 20  $\mu$ L) and tested compounds (50  $\mu$ M, 20  $\mu$ L),  $A\beta_{1-42}$  solution (50  $\mu$ M, 20  $\mu$ L) diluted by potassium phosphate buffer (50 mM, pH = 7.4, 20  $\mu$ L, DMSO content 2%) and a blank control of potassium phosphate buffer (50 mM, pH = 7.4, 20  $\mu$ L, DMSO content 2%) plus potassium phosphate buffer (50 mM, pH = 7.4, 20  $\mu$ L, DMSO content 25%). After addition and mixing, the samples above were placed in a thermostat and incubated at 37 °C for 24 h. Then, to each-well sample was added a solution (5  $\mu$ M, 160  $\mu$ L) of Thioflavin T in Glycine-NaOH buffer (50 mM, pH = 8.5), followed by shaking and scanning with a Varioskan Flash Multimode Reader for 5 min at excitation and emission wavelengths of 446 nm and 490 nm, respectively. The fluorescence value of each sample was recorded. Finally, the inhibition rate of the compounds was calculated as the formula:  $100 - (\text{Ifi-IFO})/(\text{Ic-IFO}) \times 100$ , in which the Ifi and Ifc represented the fluorescence value obtained from  $A\beta_{1-42}$  in the presence and in the absence of inhibitors, respectively, and the IFO represented the fluorescence value of the sample with only potassium phosphate buffer. In this assay, curcumin was used as a positive control and each compound was tested in three wells in parallel with each concentration.

#### 4.2.7. Disaggregation of self-induced $A\beta_{1-42}$ aggregation fibrils

For the disaggregation of self-induced  $A\beta_{1-42}$  fibrils experiment,  $A\beta_{1-42}$  solution (50  $\mu$ M, 20  $\mu$ L) and potassium phosphate buffer (20  $\mu$ L, pH = 7.4, DMSO content 25%) were first added to the 96-well plate and incubated at 37 °C for 24 h to fully aggregate the  $A\beta_{1-42}$ . Then, to the above sample was added the tested compounds (50  $\mu$ M, 20  $\mu$ L), the resulting mixture was further incubated at 37 °C for 24 h. Finally, to each-well sample was added a solution (5  $\mu$ M, 160  $\mu$ L) of Thioflavin T in Glycine-NaOH buffer (50 mM, pH = 8.5). The final concentration of both  $A\beta_{1-42}$  and the tested compounds in each well were 25  $\mu$ M. Each assay was run in triplicate. The detection method was the same as that of self-induced  $A\beta_{1-42}$  experiment.

#### 4.2.8. Inhibition of platelet aggregation

The inhibitory potencies of the tested compounds towards platelet aggregation were evaluated by the classic turbidimetric method [63,64]. First, the rats were anesthetized with chloral hydrate, and the blood was collected from their abdominal aorta, followed by anticoagulation performed with a 3.8% sodium citrate saline solution. Then, the obtained blood was centrifuged at 800 r/min for 10 min, the supernatant was carefully collected to give the desired platelet-rich plasma PRP. After that, the remaining part was further centrifuged at 3000 r/min for 15 min, and collected the supernatant to obtain the platelet-poor plasma PPP. Finally, the PRP concentration was adjusted with PPP so that the platelet count was  $6-7.5 \times 10^4/\mu\text{L}$  to obtain the required plasma. After preparing anticoagulated blood, the plasma (270  $\mu$ L) and the tested compounds (0.5 mM, 20  $\mu$ L) were added to a test cup, and incubated in the platelet aggregation apparatus at 37 °C for 5 min. Then, to the mixture above was added the induction reagent ADP solution (300  $\mu$ M, 10  $\mu$ L), and the maximum aggregation rate was tested and recorded within 5 min. The measurement was performed using physiological saline (containing 20% DMSO) instead of the tested compounds as a control group.

#### 4.2.9. In vitro antioxidant activity assay

The well-established ORAC-FL method (oxygen radical absorbance capacity by fluorescein) were used to assess the antioxidant activities of the tested compounds [65]. First, the compounds solution (10  $\mu$ M or 50  $\mu$ M, 20  $\mu$ L) and fluorescein solution (250  $\mu$ M, 120  $\mu$ L) were added to the 96-well plate. After mixing, the mixture was incubated at 37 °C for 15 min and then added 2,2'-Azobisisobutyronitrile dihydrochloride (AAPH) solution (60  $\mu$ L, 12 mM final concentration) rapidly by the automatic sampler of a Varioskan Flash Multimode Reader, followed by shaking for 30 s and measuring the fluorescence values for 90 min at

excitation and emission wavelengths of 485 nm and 535 nm, respectively. Finally, the area AUC under the fluorescence decay curve was calculated by the instrument, and the net AUC was obtained by subtracting the AUC of the blank. Trolox (6-Hydroxy-2,5,7,8-tetramethylchromane-2-carboxylic acid) was used as standard (1–8  $\mu$ M, final concentration). The blank control consisting of fluorescein (FL), potassium phosphate buffer and AAPH were performed in each assay. The antioxidant activities of the compounds were expressed as Trolox equivalents by using the standard curve calculated for each sample. All the reaction mixture was prepared in duplicate, and each set of experiment was performed independently at least three times.

#### 4.2.10. Neuroprotective activity against $H_2O_2$ -induced cell injury in PC12 cells [24,66,67]

The neuroprotection assay was conducted using PC12 cells containing 10% calf serum. First, PC-12 cells were prepared in DMEM and seeded into the 96-well plate at a density of  $1.5 \times 10^5$  cells/mL and incubated in a constant temperature incubator containing 5%  $CO_2$  at 37 °C for 24 h. After that, to the administration group was added different concentrations (1 and 10  $\mu$ M) of the tested compounds and incubated for 2 h, followed by adding  $H_2O_2$  (150  $\mu$ M) a inducer of PC12 cell injury and incubated for 24 h. Then, to the cultured PC12 cells was added MTT solution (0.5 mg/mL, 100  $\mu$ L) to measure the cell viability and cultured at 37 °C for another 2 h. Finally, DMSO (100  $\mu$ L) was added into each well to dissolve the precipitated formazan and the optical density (OD) was measured at 490 nm with a microplate reader. Results were adjusted considering OD measured in the blank. Each assay was performed independently at different concentrations in triplicate.

#### 4.2.11. In vitro anti-neuroinflammatory activity evaluation [51–53]

The anti-neuroinflammatory activity of tested compounds was evaluated through measuring their *in vitro* cytotoxicity and inhibition of LPS-induced NO and TNF- $\alpha$  production. Dulbecco's modified eagle medium (DMEM) was purchased from Gibco. Murine microglia cell line (BV-2) obtained from ATCC was cultured in DMEM and incubated at 37 °C in a humidified incubator supplemented with 5%  $CO_2$ . The inducing reagent lipopolysaccharide (LPS) was purchased from Sigma, rat TNF- $\alpha$  ELISA kit were obtained from Abcam, and nitric oxide kit was purchased from Nanjing Jiancheng Bioengineering Institute. All the tested compounds were dissolved in DMSO and diluted with PBS buffer to afford various concentrations (0.5, 2.5 and 10.0  $\mu$ M) of sample diluent before use.

*In vitro* cytotoxicity, measured by the MTT assay, was assessed through evaluating the effect of compounds on cell viability. First, BV-2 cells were seeded in DMEM (100  $\mu$ L) and cultured in 96-well cell culture microplate and incubated in a humidified incubator containing 5%  $CO_2$  at 37 °C for 24 h. Then, 10  $\mu$ L of tested samples (0.5, 2.5 and 10.0  $\mu$ M) were added to cells in triplicate wells and a blank control group was set, followed by incubation for another 30 min. Subsequently, the treated cells were exposed to LPS (1.0  $\mu$ g/mL, 10  $\mu$ L) and continued the culture for 24 h, and MTT (3-(4,5-dimethylthiazol-2-yl)-2,5-diphenyltetrazolium bromide) solution (0.5 mg/mL, 10  $\mu$ L), dissolved with PBS buffer, was added to each well and incubated for 4 h at 37 °C. Finally, the crystals obtained were dissolved in DMSO (200  $\mu$ L) and OD values were measured at 490 nm using a spectrophotometer. The results were recorded and expressed as the percent cell viability compared to the control group.

Griess reagent system, following the manufacturers' protocols, was used to evaluate the inhibition of LPS-induced NO production. The methods of culturing BV-2 cells, setting blank control and adding tested compounds and LPS were the same as those in cytotoxicity assay. After that, the cell culture supernatants and different concentrations of  $NaNO_2$  as a standard were added to a 96-well plate since the  $NaNO_2$  concentration in the supernatant could act as an indicator of NO production. Then, to each well was added the same volume of Griess reagent and incubated at room temperature for 10 min. Finally, the absorbance was

monitored at 540 nm using an ELISA plate reader to measure the results of NO production.

Inhibition of LPS-induced TNF- $\alpha$  production was evaluated with an enzyme-linked immunosorbent assay (ELISA). The methods of BV-2 cells culture, adding different concentration of tested compounds (10  $\mu$ L) and LPS (1.0  $\mu$ g/mL, 10  $\mu$ L) and setting blank control group were the same as above in cytotoxicity assay. Then, the supernatant of the cell culture solution (50  $\mu$ L) was added to a 96-well plate and the release of cytokine TNF- $\alpha$  was measured by ELISA according to the instructions of the ELISA kit.

#### 4.2.12. *In vitro* blood–brain barrier permeation assay

The parallel artificial membrane permeation assay of the blood–brain barrier (PAMPA-BBB) reported by Di *et al.* was performed to measure the BBB permeability of the selected compounds **15b** and **16b** [54]. First, the porcine brain lipid (PBL) was dissolved in dodecane (20 mg/mL) to be a mixing solution, of which 4  $\mu$ L was dropped on the lipophilic filter membrane of the receptor hole to simulate the biofilm. After standing for 5 min, the evenly infiltrated hydrophobic film changed from white to translucent. Then, to the donor microplate was added the tested compounds (100  $\mu$ g/mL, 350  $\mu$ L), and the acceptor microplate was filled with 300  $\mu$ L of PBS/EtOH (7:3) so that the phospholipid membrane could touch the donor fluid, thus forming a sandwich-like structure with the donor solution at the bottom. After that, the sandwich-like structure was placed in a humidified environment at 25  $^{\circ}$ C for 18 h, followed by removing the donor microplate, adding the solution above (150  $\mu$ L) in the acceptor and donor wells to the quartz 96-well plate, respectively, scanning at 200–600 nm (step = 10 nm) with the Varioskan Flash Multimode Reader (Thermo Scientific), and finally recording the OD values. Each assay was performed independently in triplicate. The concentrations of tested compounds in the donor and acceptor wells were measured and the effective transmittance ( $P_e$ ) was calculated by the following formula:  $P_e = -\ln [1 - C_A(t)/C_{\text{equilibrium}}]/[A \times (1/V_D + 1/V_A) \times t]$ ,  $C_{\text{equilibrium}} = [C_D(t) \times V_D + C_A(t) \times V_A]/(V_D + V_A)$ , in which  $C_A(t)$  represented the concentration of the receptor fluid at the time of  $t$ ,  $A$  represented the area of artificial phospholipid membrane ( $A = 0.28 \text{ cm}^2$ ),  $t$  represented the permeation time,  $V_A$  represented the volume of the donor pore,  $V_D$  represented the volume of the receptor pore and  $C_D(t)$  represented the concentration of donor fluid at the time of  $t$ . In this experiment, the BBB permeability of 11 commercial drugs were detected to validate the assay. Each sample was analyzed at ten wavelengths in four wells and the results were expressed as mean  $\pm$  SD.

#### Declaration of Competing Interest

The authors declare that they have no known competing financial interests or personal relationships that could have appeared to influence the work reported in this paper.

#### Acknowledgments

This work was supported by Chinese National Natural Science Foundation (22077091), Sichuan Science and Technology Program (2020YFS0067) and the Fundamental Research Funds for the Central Universities.

#### Appendix A. Supplementary data

Supplementary data to this article can be found online at <https://doi.org/10.1016/j.bioorg.2021.104895>.

#### References

- [1] Alzheimer's Association, Alzheimer's disease facts and figures, *Alzheim. Dement.* 15 (2019) (2019) 321–387.

- [2] J. Godyř, J. Jończyk, D. Panek, Therapeutic strategies for Alzheimer's disease in clinical trials, *Pharmacol. Rep.* 68 (2016) 127–138.
- [3] E. Sara, B. Jem, C. Adelina, World Alzheimer report 2019: Attitudes to dementia, (2019) 1–16.
- [4] S. Piyooosh, S. Pavan, S. Ankit, Comprehensive review of mechanisms of pathogenesis involved in Alzheimer's disease and potential therapeutic strategies, *Prog. Neurobiol.* 174 (2019) 53–89.
- [5] T. Ahmed, S. Zahid, A. Mahboob, Cholinergic system and post-translational modifications: an insight on the role in Alzheimer's disease, *Curr. Neuropharmacol.* 15 (2017) 480–494.
- [6] I. Silman, J.L. Sussman, Acetylcholinesterase: "classical" and "non-classical" functions and pharmacology, *Curr. Opin. Pharmacol.* 5 (2005) 293–302.
- [7] D. Galimberti, E. Scarpini, Old and new acetylcholinesterase inhibitors for Alzheimer's disease, *Expert. Opin. Investig. Drugs* 25 (2016) 1–7.
- [8] L.Y. Fan, M.J. Chiu, Comorbidity and current concepts as well as future strategies for the treatment of Alzheimer's disease, *Neuropsychiatr. Dis. Treat.* 10 (2014) 439–451.
- [9] M. Rosini, E. Simoni, R. Caporaso, A. Minarini, Multitarget strategies in Alzheimer's disease: benefits and challenges on the road to therapeutics, *Fut. Med. Chem.* 6 (2016) 697–711.
- [10] P. Zhang, Multi-target design strategies for the improved treatment of Alzheimer's disease, *Eur. J. Med. Chem.* 176 (2019) 228–247.
- [11] Z.Y. Cai, Monoamine oxidase inhibitors: promising therapeutic agents for Alzheimer's disease, *Mol. Med. Rep.* 9 (2014) 1533–1541.
- [12] F. Caraci, A. Copani, F. Nicoletti, F. Drago, Depression and Alzheimer's disease: neurobiological links and common pharmacological targets, *Eur. J. Pharmacol.* 626 (2010) 64–71.
- [13] R.A. Himes, G.Y. Park, G.S. Siluvai, N.J. Blackburn, K.D. Karlin, Structural studies of copper (I) complexes of amyloid-beta peptide fragments: formation of two-coordinate bis(histidine) complexes, *Angew. Chem.* 47 (2008) 9084–9087.
- [14] H. Zheng, T. Amit, O. Bar-Am, M. Fridkin, M.B. Youdim, S.A. Mandel, From anti-Parkinson's drug rasagiline to novel multitarget iron chelators with acetylcholinesterase and monoamine oxidase inhibitory and neuroprotective properties for Alzheimer's disease, *J. Alzheimers Dis.* 30 (2012) 1–16.
- [15] T. Mohamed, A. Shakeri, P.P.N. Rao, Amyloid cascade in Alzheimer's disease: recent advances in medicinal chemistry, *Eur. J. Med. Chem.* 113 (2016) 258–272.
- [16] Justin M. Long, D.M. Holtzman, Alzheimer Disease: An Update on Pathobiology and Treatment Strategies, *Cell* 179 (2019) 312–339.
- [17] A. Jan, O. Gokce, R. Luthi-Carter, H.A. Lashuel, The ratio of monomeric to aggregated forms of A $\beta$ 40 and A $\beta$ 42 is an important determinant of amyloid- $\beta$  aggregation, fibrillogenesis, and toxicity, *J. Biol. Chem.* 42 (2008) 28176–28189.
- [18] S. Cattricala, M. Torti, G. Ricevuti, Alzheimer disease and platelets: how's that relevant, *Immun. Ageing* 9 (2012) 20.
- [19] L. Donner, K. Falkner, L. Gremer, Platelets contribute to amyloid- $\beta$  aggregation in cerebral vessels through integrin  $\alpha_{\text{IIb}}\beta_3$ -induced outside-in signaling and clusterin release, *Sci. Signal.* 9 (2016) 429–495.
- [20] G. Azizi, A. Mirshafiey, The potential role of proinflammatory and anti-inflammatory cytokines in Alzheimer disease pathogenesis, *Immunopharm. Immunot.* 34 (2012) 881–895.
- [21] B.L.O. De, P. Bellozi, H.J. Reis, Inflammation as a possible link between dyslipidemia and Alzheimer's disease, *Neuroscience* 376 (2018) 127–141.
- [22] A. Michelucci, T. Heurtaux, L. Grandbarbe, Characterization of the microglial phenotype under specific pro-inflammatory and anti-inflammatory conditions: effects of oligomeric and fibrillar amyloid- $\beta$ , *J. Neuroimmunol.* 210 (2009) 3–12.
- [23] G.P. Cortese, C. Burger, Neuroinflammatory challenges compromise neuronal function in the aging brain: Postoperative cognitive delirium and Alzheimer's disease, *Behav. Brain. Res.* 322 (2016) 269–279.
- [24] B.L. Jalili, H. Nadri, A. Moradi, New racemic annulated pyrazolo[1,2-b]phthalazines as tacrine-like AChE inhibitors with potential use in Alzheimer's disease, *Eur. J. Med. Chem.* 139 (2017) 280–289.
- [25] N. Vila, P. Besada, T. Costas, Phthalazin-1(2H)-one as a remarkable scaffold in drug discovery, *Eur. J. Med. Chem.* 97 (2015) 462–482.
- [26] J. Sangshetti, S.K. Pathan, R. Patil, S.A. Ansari, S. Chhajed, R. Arote, D.B. Shinde, Synthesis and biological activity of structurally diverse phthalazine derivatives: A systematic review, *Bioorg. Med. Chem.* 27 (2019) 3979–3997.
- [27] L. Luo, Q. Song, Y. Li, Z.Z. Cao, X.M. Qiang, Z.H. Tan, Y. Deng, Design, synthesis and evaluation of phthalide alkyl tertiary amine derivatives as promising acetylcholinesterase inhibitors with high potency and selectivity against Alzheimer's disease, *Bioorg. Med. Chem.* 28 (2020) 115–400.
- [28] P.A. Peixoto, A. Jean, J. Maddaluno, Formal enantioselective synthesis of aplykurodinone-1, *Angew. Chem., Int. Ed.* 52 (2013) 6971–6973.
- [29] L.L. De, G. Giacomelli, A. Porcheddu, A mild and efficient alternative to the classical Swern oxidation, *J. Org. Chem.* 66 (2001) 7907–7909.
- [30] X.M. Qiang, Y. Li, X. Yang, L. Luo, R. Xu, Y.X.Z. Zheng, Z.Z. Cao, Z.H. Tan, Y. Deng, DL-3-n-butylphthalide-Edaravone hybrids as novel dual inhibitors of amyloid- $\beta$  aggregation and monoamine oxidases with high antioxidant potency for Alzheimer's therapy, *Bioorg. Med. Chem. Lett.* 27 (2017) 718–722.
- [31] O.O. Kolodyazhnaya, O.I. Kolodyazhnyi, R.A. Cherkasov, Synthesis of  $\alpha$ -hydroxy (polyprenyl) bisphosphonates, *Russ. J. Gen. Chem.* 84 (2014) 647–653.
- [32] A. Pankova, M. Kuznetsov, M. Sorokina, Thermal rearrangement of 2,3-diaryl-1-phthalimidoaziridines, *Tetrahedron Lett.* 56 (2015) 5381–5385.
- [33] E.D. Olmo, B.M. Barboza, Vasorelaxant activity of phthalazinones and related compounds, *Bioorg. Med. Chem. Lett.* 16 (2006) 2786–2790.
- [34] J. Zhang, H. Zhang, W. Cai, 'Click' D<sub>1</sub> receptor agonists with a 5-HT<sub>1A</sub> receptor pharmacophore producing D<sub>2</sub> receptor activity, *Bioorg. Med. Chem.* 17 (2009) 4873–4880.

- [35] J. Epszajn, J.Z. Brzeziński, K. Czech, Application of organolithium and related reagents in synthesis. Part XII. Synthesis of phenyl- and pyridylpyridopyridazinones and their derivatives, *Monats. Chem.* 124 (1993) 549–558.
- [36] S. Xu, C. Li, X. Jia, AlCl<sub>3</sub>-promoted selective michael addition with allenolate and methyleneindolinone: synthesis of spirocyclic oxindole by using allenolate as a four-carbon component building block, *J. Org. Chem.* 79 (2014) 11161–11169.
- [37] C. Niebel, V. Lokshin, M. Sigalov, Intra- and intermolecular C(sp<sup>2</sup>)-H...O hydrogen bonds in a series of isobenzofuranone derivatives: manifestation and energetics, *Eur. J. Org. Chem.* 21 (2008) 3689–3699.
- [38] M. Agrawal, P. Kharkar, S. Moghe, Discovery of thiazolyl-phthalazinone acetamides as potent glucose uptake activators via high-throughput screening, *Bioorg. Med. Chem. Lett.* 23 (2013) 5740–5743.
- [39] M. Mautino, S. Kumar, J. Waldo, Fused imidazole derivatives useful as IDO inhibitors, US9388191 (2016).
- [40] Z.H. Shi, N.G. Li, Q.P. Shi, Synthesis of scutellarein derivatives to increase biological activity and water solubility, *Bioorg. Med. Chem.* 23 (2015) 6875–6884.
- [41] Y. Li, X.M. Qiang, L. Luo, Multitarget drug design strategy against Alzheimer's disease: Homoisoflavonoid Mannich base derivatives serve as acetylcholinesterase and monoamine oxidase B dual inhibitors with multifunctional properties, *Bioorg. Med. Chem.* 25 (2017) 714–726.
- [42] X. Zhang, Q. Song, Z. Cao, Design, synthesis and evaluation of chalcone mannich base derivatives as multifunctional agents for the potential treatment of Alzheimer's disease, *Bioorg. Chem.* 87 (2019) 395–408.
- [43] Y. Li, X.M. Qiang, L. Luo, Synthesis and evaluation of 4-hydroxyl aurone derivatives as multifunctional agents for the treatment of Alzheimer's disease, *Bioorg. Med. Chem.* 24 (2016) 2342–2351.
- [44] M. Bartolini, C. Bertucci, M.L. Bolognesi, Insight into the kinetic of amyloid  $\beta$  (1–42) peptide self-aggregation: elucidation of inhibitors' mechanism of action, *ChemBioChem.* 8 (2007) 2152–2161.
- [45] A. Sugimoto, K. Sakamoto, Y. Fujino, Synthesis and inhibitory effect on platelet aggregation of 2-phenyl-1(2*H*)-phthalazinone derivatives, *Chem. Pharm. Bull.* 17 (1985) 2809–2820.
- [46] Y. Eguchi, F. Sasaki, Y. Takashima, Studies on antiatherosclerotic agents. synthesis of 7-ethoxycarbonyl-4-formyl-6,8-dimethyl-1(2*H*)-phthalazinone derivatives and related compounds, *Chem. Pharm. Bull.* 39 (1991) 795–797.
- [47] X. Ning, Y. Guo, X. Ma, Design, synthesis and pharmacological evaluation of (*E*)-3,4-dihydroxy styryl sulfonamides derivatives as multifunctional neuroprotective agents against oxidative and inflammatory injury, *Bioorg. Med. Chem.* 21 (2013) 5589–5597.
- [48] G.C. Brown, A. Bal-Price, Inflammatory neurodegeneration mediated by nitric oxide, glutamate and mitochondria, *Mol. Neurobiol.* 27 (2003) 325–355.
- [49] M.H. Ahmad, M. Fatima, A.C. Mondal, Influence of microglia and astrocyte activation in the neuroinflammatory pathogenesis of Alzheimer's disease: rational insights for the therapeutic approaches, *J. Clin. Neurosci.* 59 (2019) 6–11.
- [50] F.L. Heppner, R.M. Ransohoff, B. Becher, Immune attack: the role of inflammation in Alzheimer disease, *Nat. Rev. Neurosci.* 6 (2015) 358–372.
- [51] E. Taka, E.A. Mazzi, C.B. Goodman, N. Redmon, H. Flores-Rozas, R. Reams, S. Darling-Reed, K.F. Soliman, Anti-inflammatory effects of thymoquinone in activated BV-2 microglial cells, *J. Neuroimmunol.* 286 (2015) 5–12.
- [52] Z.Z. Cao, J. Yang, R. Xu, Q. Song, X.Y. Zhang, H.Y. Liu, X.M. Qiang, Y. Li, Z.H. Tan, Y. Deng, Design, synthesis and evaluation of 4'-OH-flurbiprofen-chalcone hybrids as potential multifunctional agents for Alzheimer's disease treatment, *Bioorg. Med. Chem.* 5 (2018) 1102–1115.
- [53] D. Tweedie, W. Luo, R.G. Short, A. Bossi, H.W. Holloway, Y. Li, Q.S. Yu, N. H. Greig, A cellular model of inflammation for identifying TNF- $\alpha$  synthesis inhibitors, *J. Neurosci. Meth.* 2 (2009) 182–187.
- [54] L. Di, E.H. Kerns, K. Fan, High throughput artificial membrane permeability assay for blood-brain barrier, *Eur. J. Med. Chem.* 38 (2003) 223–232.
- [55] K.S. Achintya, T.B. Ronald, General method for the synthesis of phthalaldehydic acids and phthalides from *o*-bromobenzaldehydes via ortho-lithiated aminoalkoxides, *J. Org. Chem.* 48 (1983) 2356–2360.
- [56] H.J. Kumpaty, J.S. Williamson, S. Bhattacharyya, Synthesis of *N*-methyl secondary amines, *Synth. Commun.* 33 (2003) 1411.
- [57] S. Kang, S. Lee, W. Yang, A direct assay of butyrylcholinesterase activity using a fluorescent substrate, *Org. Biomol. Chem.* 14 (2016) 8815–8820.
- [58] M.V. Sigalov, E.P. Doronina, V.F. Sidorkin, C<sub>Ar</sub>-H...O hydrogen bonds in substituted isobenzofuranone derivatives: geometric, topological, and NMR characterization, *J. Phys. Chem. A.* 116 (2012) 7718–7725.
- [59] L. Luo, Y. Li, X.M. Qiang, Multifunctional thioxanthone derivatives with acetylcholinesterase, monoamine oxidases and  $\beta$ -amyloid aggregation inhibitory potencies as potential agents against Alzheimer's disease, *Bioorg. Med. Chem.* 25 (2017) 1997–2009.
- [60] N. Desideri, A. Bolasco, R. Fioravanti, Homoisoflavonoids: natural scaffolds with potent and selective monoamine oxidase-B inhibition properties, *J. Med. Chem.* 54 (2011) 2155–2164.
- [61] M. Rosini, E. Simoni, M. Bartolini, Inhibition of acetylcholinesterase, beta-amyloid aggregation, and NMDA receptors in Alzheimer's disease: A promising direction for the multi-target-directed ligands gold rush, *J. Med. Chem.* 51 (2008) 4381–4384.
- [62] R.S. Li, X.B. Wang, X.J. Hu, Design, synthesis and evaluation of flavonoid derivatives as potential multifunctional acetylcholinesterase inhibitors against Alzheimer's disease, *Bioorg. Med. Chem. Lett.* 23 (2013) 2636–2641.
- [63] C.C. Wu, T.W. Wang, W.Y. Wang, 2-(2-*Br*-phenyl)-8-methoxy-benzoxazinone (HPW-RX2), a direct thrombin inhibitor with a suppressive effect on thromboxane formation in platelets, *Eur. J. Pharmacol.* 527 (2005) 37–43.
- [64] G.V. Born, M.J. Cross, The aggregation of blood platelets, *J. Physiol.* 168 (1963) 178–195.
- [65] L. Fang, B. Kraus, J. Lehmann, Design and synthesis of tacrine-ferulic acid hybrids as multi-potent anti-Alzheimer drug candidates, *Bioorg. Med. Chem. Lett.* 18 (2008) 2905–2909.
- [66] P. Xu, K.Z. Wang, C. Lu, L.M. Dong, Protective effect of lavender oil on scopolamine induced cognitive deficits in mice and H<sub>2</sub>O<sub>2</sub> induced cytotoxicity in PC12 cells, *J. Ethnopharmacol.* 193 (2016) 408–415.
- [67] Z.Y. Yang, Q. Song, Z.Z. Cao, Design, synthesis and evaluation of flurbiprofen-cloquinol hybrids as multitarget-directed ligands against Alzheimer's disease, *Bioorg. Med. Chem.* 28 (2020) 115–374.